 70-2314

HORWEDEL, Jon Harold, 1942-
AN APPLICATION OF PATTERN RECOGNITION THEORY TO WEATHER PREDICTION USING QUANTIZED RADAR DATA.

The University of Oklahoma, Ph.D., 1969
Engineering, electrical

University Microfilms, Inc., Ann Arbor, Michigan

THE UNIVERSITY OF OKLAHOMA

GRADUATE COLLEGE

AN APPLICATION OF PATTERN RECOGNITION THEORY TO WEATHER PREDICTION USING QUANTIZED RADAR DATA

A DISSERTATION

SUBMITTED TO THE GRADUATE FACULTY

in partial fulfillment of the requirements for the

degree of

DOCTOR OF PHILOSOPHY

BY

JON HAROLD HORWEDEL

Norman, Oklahoma

1969

AN APPLICATION OF PATTERN RECOGNITION THEORY TO WEATHER PREDICTION USING QUANTIZED RADAR DATA

APPROVED BY

W J Kuriger

G B Walker

S. K. Kahng

Gerald Tuma

George M. Ewing

DISSERTATION COMMITTEE

ACKNOWLEDGEMENT

The author wishes to express his gratitude to the Faculty of the School of Electrical Engineering and others at the University of Oklahoma for their assistance in preparing this work. The author also wishes to express his grateful appreciation to Dr. William L. Kuriger, under whose direction and council this thesis was prepared. The advice and assistance of Mr. Kenneth Wilk and Dr. Edwin Kessler of the National Severe Storms Laboratory, Norman, Oklahoma, is also greatly appreciated.

Special thanks are extended to the National Aeronautics and Space Administration and to the Graduate College, University of Oklahoma, for their support and assistance.

TABLE OF CONTENTS

LIST OF TABLES

LIST OF ILLUSTRATIONS

AN APPLICATION OF PATTERN RECOGNITION THEORY TO WEATHER PREDICTION USING QUANTIZED RADAR DATA

CHAPTER I

INTRODUCTION

Pattern recognition techniques have been applied to a variety of useful applications: character recognition, speech identification, and electro-cardiogram diagnosis. But the increasingly important need for short-term weather prediction has received little attention. An automatic short-term weather forecasting system will certainly be an integral part of future automated air traffic control. Until recently the data obtained about the small scale features of the weather was already hours old before it could be reduced to a form suitable for automatic prediction. The National Severe Storms Laboratory, Norman, Oklahoma, a division of the United States Department of Commerce's Environmental Science Services Administration, has devised a procedure for recording on magnetic tape the weather information contained in a normal plan position indicator (PPI) radar scan minutes after it occurs (25).

Having overcome the problem of suitable data acquisition, the next step is the formulation of a workable prediction scheme. Although a prediction plan has already been proposed (22), it is only a first order approach to the problem and neglects important features of the weather that could be used for prediction. The short-term weather prediction scheme to be presented in this paper extends and modifies the earlier plan and, for this reason, may be regarded as a second order approach. Although each part of the proposed prediction plan has a theoretical foundation, the manner in which the parts are interconnected classifies the entire scheme as heuristic.

A review of the fundamentals of radar meteorology and the method used by the National Severe Storms Laboratory to obtain the digitized weather data will be discussed. The purpose for presenting this meteorological material is twofold. First, because of the interdisciplinary approach to solving the problem of short-term weather prediction, it is necessary for those not having a background in meteorology. Secondly, necessary definitions must be presented in order that they may be referred to throughout the study.

After establishing a meteorological foundation, a development of the already known prediction plan is presented. Several modifications of the proposed plan are discussed and the results tabulated for two actual storms. By comparing the several schemes used, it is hoped that a firm basis will be established from which future automated forecasting schemes can be devised.

CHAPTER II

RADAR METEOROLOGY

The Equivalent Radar Reflectivity Factor

In the application of radar to detect meteorological phenomena, the basic radar equation is modified and a new term, equivalent radar reflectivity factor Z_e, is defined. The basic radar equation is

$$P_r = \frac{P_t G^2 \lambda^2 \sigma}{64\pi^3 R^4} \quad , \tag{2.1}$$

where

P_r - Echo power received
P_t - Power transmitted
R - Range of target
G - Antenna gain
σ - Radar cross section of target
λ - Wavelength

Equation 2.1 gives the echo power returned from a single target of radar cross section σ. The radar cross section σ is not the physical cross section of the target, but is the "backscattering cross section". It is defined as "the area intercepting that amount of power which, if scattered isotropically, would return to the receiver an amount of power equal to that actually received" (1). However in the case of meteorological targets, such as rain, snow, and hail, there are a large number of independent scatterers. If there are N particles per unit volume and the radar cross section of the i th particle is σ_i, then the average total backscatter cross section per unit volume is $\sum_i^N \sigma_i$. The total radar cross section may be expressed as $V_m \sum_i^N \sigma_i$, where V_m is the volume that the radar beam can effectively illuminate.

A radar with vertical beamwidth φ_B, horizontal beamwidth θ_B, and pulse duration time τ, will illuminate a volume at any instant that can be approximated by an elliptic cylinder. If c is the velocity of propagation, then the length of the radar pulse in space is $h = c\tau$. The power backscattered by particles at range $(R + h/2)$ from the leading edge of the pulse will arrive at the antenna at the same time as energy backscattered by particles at range R from the trailing edge of the pulse; therefore the depth of the volume is h/2. Hence, the volume illuminated is

$$V_m = \pi(\frac{\varphi_B}{2} R) \ (\frac{\theta_B}{2} R) \ \frac{h}{2} \ . \tag{2.2}$$

Because of the motion of the precipitation particles relative to each other and the motion of the particles as a whole relative to the radar set, there is considerable variation of the received energy from pulse to pulse. Slowing the scan rate and taking the average of the returned power results in a smoothing of the signal fluctuation from these random motions. By using the approximate relation, $G \approx 4\pi/\varphi_B \theta_B$, the average received power may be written

$$\overline{P}_r = \frac{P_t G \lambda^2 h}{128\pi R^2} \sum_{i=1}^{N} \sigma_i \ . \tag{2.3}$$

If the wavelength is much greater than the circumference of a scattering particle of diameter D_i (Rayleigh scattering region), it can be shown (p. 27, Batten) that the radar cross section is

$$\sigma_i = \frac{\pi^5 D_i^{\ 6}}{\lambda^4} |K|^2 \ . \tag{2.4}$$

The constant $|K|^2$ depends on the wavelength and the dielectric constant of the scatterer. For λ = 10cm, the value for water at 10^oC is approximately 0.93, while $|K|^2$ for ice is about 0.197. When ice acquires a thin coating of water, the value for $|K|^2$ is almost that of an all water particle (1). Hence the value for $|K|^2$ can be considered a constant for summer precipitation.

Substituting Equation 2.4 in Equation 2.3, the average received power is

$$\overline{P}_r = \frac{P_t G h \pi^4}{128\ \lambda^2 R^2} \left|K\right|^2 \sum_{i=1}^{N} D_i^{\,6} \ . \tag{2.5}$$

The radar reflectivity factor Z is defined as $\sum_i^N D_i^{\,6}$ ($mm^6\ m^{-3}$) and is a measure of particle size and distribution. Equation 2.5 then becomes

$$\overline{P}_r = \frac{C}{R^2}\ Z \ , \tag{2.6}$$

where C is a constant for a particular radar and precipitation situation. Equation 2.5 shows that the return power is dependent on the size of the scattering particles and the range. After range-square normalization, the return power is directly proportional to the size of the scatterers. Hence, the return energy is a measure of the size and distribution of the precipitation particles.

Equation 2.6 was derived for scatterers in the Rayleigh region. However by a slight modification, the equation can be made applicable for all regions of meteorological interest. By summing both sides of Equation 2.3 over all particles and then rearranging, the reflectivity factor is

$$Z = \frac{\lambda^4}{\pi^5 \left|K\right|^2} \sum_{i=1}^{N} \sigma_i \ . \tag{2.7}$$

Outside the Rayleigh scattering region, Equation 2.7 can be used to define an equivalent radar reflectivity factor Z_e. The defining equation for Z_e is

$$Z_e = \frac{\lambda^4}{\pi^5 \left|K\right|^2} \sum_{i=1}^{N} \sigma_i \ . \tag{2.8}$$

The equivalent radar reflectivity factor is defined as "the reflectivity factor associated with Rayleigh scatterers having the same radar cross section as the actual scatterers" (8). After rearrangement, Equation 2.8 becomes

$$\sigma_i = \frac{\pi^5 |K|^2}{\lambda^4} Z_e . \tag{2.9}$$

Substituting Equation 2.9 into Equation 2.3 allows the average return power to be written as

$$\overline{P}_r = \frac{P_t G \pi^4 h}{128 \lambda^2 R^2} |K|^2 Z_e . \tag{2.10}$$

Hence,

$$\overline{P}_r = \frac{C}{R^2} Z_e . \tag{2.11}$$

Since Z_e is a measure of particle size and is not confined to the Rayleigh scattering region, the average received echo power is a measure of the particle size and number for all regions of interest.

The WSR-57 Weather Radar Installation

The WSR-57 radar installation at the National Severe Storms Laboratory located in Norman, Oklahoma, is essentially the same as many United States Weather Bureau stations. The characteristics of the National Severe Storms Laboratory radar is summarized in Table 2.1 (21).

The radar transmitter and receiver circuits are mounted on the drive pedestal with the antenna in an air conditioned fiberglass radome atop a 75 foot tower. The radar is a conventional non-coherent system using a balanced mixer and a low noise preamplifier. A block diagram of the radar installation is shown in Figure 2.1 (21). A sensitivity time control (STC) bias provides inverse range-squared intensity normalization to an accuracy of 1 db for targets between 20 and 100 nautical miles. Because of the extreme range of signals for meteorological targets, the range normalized signal is applied to an IF amplifier with the logarithmic

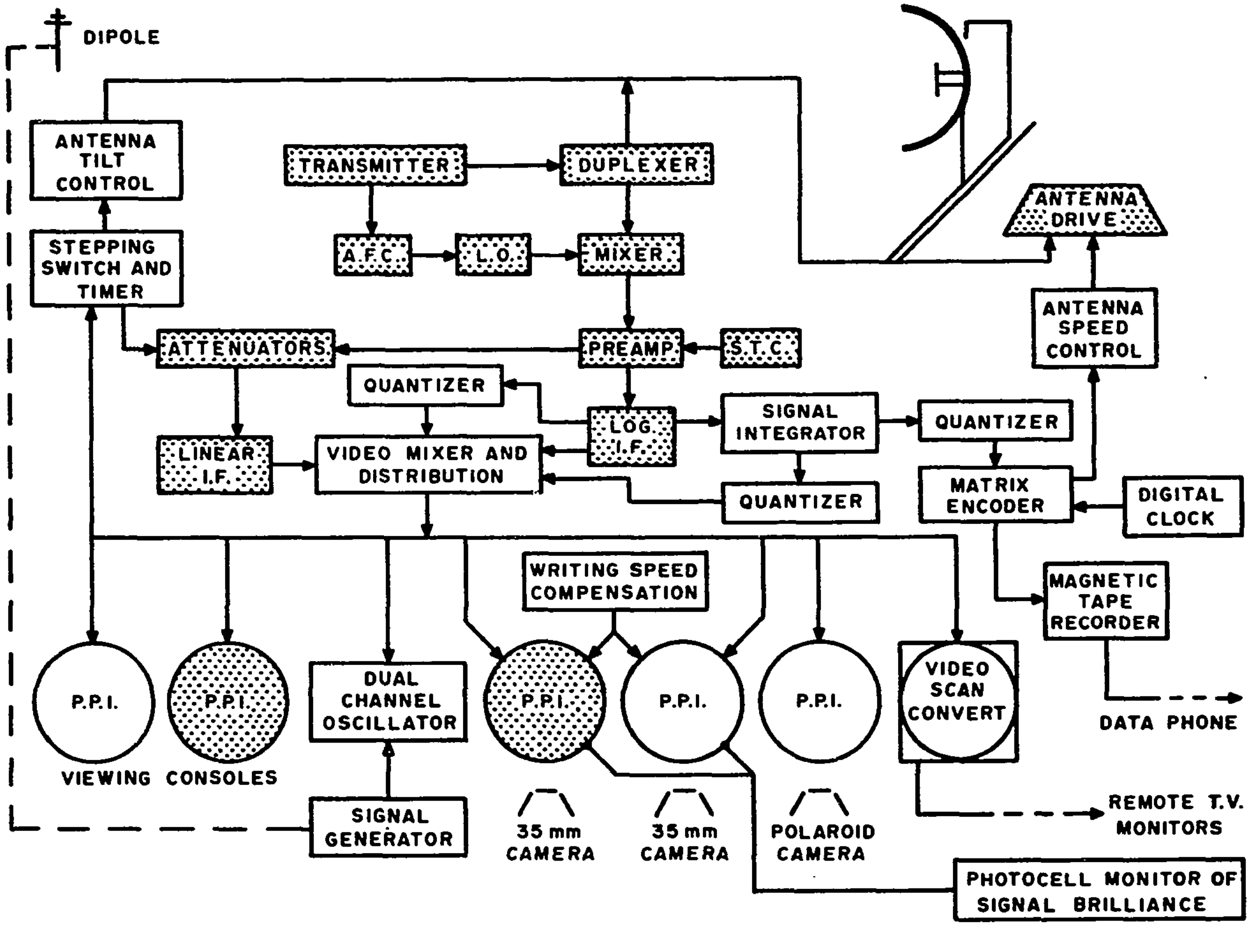

Figure 2.1. Block diagram of the radar installation at the National Severe Storms Laboratory. The shaded areas constitute the basic radar.

characteristics required for accurate output voltage representation of unattenuated signals.

TABLE 2.1

CHARACTERISTICS OF THE WSR-57 RADAR INSTALLATION AT THE NATIONAL SEVERE STORMS LABORATORY

Wavelength	10 cm.
Peak Power	450 kw.
Pulse length	4 μsec.
Pulse repetition frequency	164 per sec.
Minimum detectable signal	-110 dbm*
Beamwidth	2 deg.
Antenna gain	38.5 db
Azimuthal scan rate	2 rpm for PPI display .45 rpm for magnetic tape

* The threshold signal choosen for display is -104 dbm, corresponding to $Z_e = 10\ mm^6\ m^{-3}$ at 100 nautical miles.

The video output of the logarithmic amplifier is sent to a signal integrator for averaging before quantization. The log video passes through an amplifier whose output is integrated into 200 range intervals of 0.65 nautical miles each. The processing range of 131 nautical miles may be adjusted to the location of echoes of greatest interest. For this study the range of interest was 20 to 100 nautical miles; therefore, the processing range was 20 to 151 nautical miles. The outputs of the integrators are fed to a digital translator for recording on magnetic tape.

The function of the digital translator is to provide the necessary circuitry to convert the information contained in the integrated video to a suitable form for storage on magnetic tape. A record is made of the integrated video for each two degrees of azimuthal antenna rotation. Each record is divided into eighty range intervals of 1.375 nautical miles each. The signal representing each interval is quantized into seven levels and encoded by a BCD matrix for storage on magnetic tape.

Since a complete plan position indicator (PPI) scan contains 180 records, the entire scan contains 14,400 discrete video samples. The quantized levels are referenced to the logarithm of the equivalent radar reflectivity factor; therefore, the recorded values are log Z_e truncated to the lower whole number.

Auxiliary circuits provide observation time in digital format and automatic control of antenna rotation. The antenna must be slowed from its normal rate of 2 rpm to below 0.45 rpm when data is being recorded on magnetic tape.

The first quadrant of a B-scan digital output is shown in Figure 2.2. The B-scan configuration has range as abscissa and azimuth as ordinate. The first four digits in the first record (the north azimuth) is the time of the start of the radar scan. The remaining digits in the first line refer to the categories of the equivalent radar reflectivity factor Z_e in range steps of 1.375 nautical miles. The following 179 lines complete the PPI scan. Line number 181 contains the time for the start of the next scan. A new scan may be started every 140 seconds; however, for this study a new scan was started every fifteen minutes.

Conversion to Rectangular Form

The range-azimuth form of the B-scan configuration is not readily applicable to prediction calculations. The intensity categories of the B-scan represent different areas. For the prediction method used in this study, it is desirable that each intensity category be a measure of the equivalent radar reflectivity factor for equal areas. A conversion is performed that changes the polar form of the B-scan to rectangular or square form.

Several rectangular patterns are given in Appendix C. The pattern shown in Figure C.3 is the rectangular pattern for the partial B-scan of Figure 2.2. The entire rectangular pattern contains 6,400 squares, each representing an area of 6.25 square nautical miles. Only those intensity categories for range locations between 20 and 100 nautical miles are considered. This is the optimum range of the radar installation (2) and involves 10,800 points of the original B-scan. There are 4,948 squares of the rectangular pattern that represent the optimum range. The

```
14270000000000000000233442000002321000000000000000000000000000000000000000000000000
00000000000000000000133443201334433200000000000000001000000000000000000000000000000
00000000000000000000122443334444333200000000000001000000000000000000000000000000000
00000000000000000000002444344444442100000000000002200000000000000000000000000000000
00000000000000000000002333333333333322100000000000000000000000000000000000000000000
00000000000000000000000223333333333333322111000003322110000000000000000000000000000
00000000000000000000000122223324433443222220000233222100000000000000000000000000000
00000000000000000000000121123324443333322222211000000000000000000000000000000000000
00000000000000000000000000000000000000000000000000000000000000000000000000000000000
```

FIGURE 2.2. FIRST QUADRANT OF B-SCAN FOR 1427 CST, MAY 13, 1967

remaining 1,452 squares represent area outside the optimum range and are designated as X's in the rectangular patterns.

Because of the reduction in the number of data points, the conversion from B-scan to rectangular form results in an averaging of the original data. Each intensity category of the B-scan represents the logarithm of the reflectivity factor for an area whose shape is a portion of a circular sector. These B-scan areas vary from 1.0 square nautical miles at 20 nautical miles to 4.9 square nautical miles at 100 nautical miles. A square of the rectangular pattern has area in common with several of these circular areas. If $A_1, A_2, \ldots, A_n$ are the areas that the B-scan has in common with a given square and if $I_1, I_2, \ldots, I_n$ are the associated intensity categories, then the intensity category I for the square is given by

$$I = \left\lceil \mathrm{Log}\left\{ \sum_{i=1}^{n} \frac{A_i \cdot 10^{I_i}}{6.25} \right\} + K \right\rceil \tag{2.12}$$

where $\lceil X \rceil$ denotes "the largest integer less than or equal to X." The constant K can be empirically chosen for proper weighting of the intensity categories. For this study, K was chosen so that the percentage of total area covered by a nonzero intensity category is approximately the same for both the B-scan and the rectangular pattern. The value of K used was 0.3979400. This choice of K also leads to another interpretation. If 30% or more of the area of a square is covered by an intensity category and 70% or less is covered by the next lower intensity category, then the larger intensity category is chosen for the square.

The Radar Reflectivity Factor as a Measure of Severe Weather

The equivalent reflectivity factor can be used as a measure of severe weather. Several studies (1,8,9,10,17,19) have been made indicating a direct correlation between high reflectivity factors and severe weather. Equally important, there is also a direct correlation between low reflectivity factors and an absence of severe weather. As indicated before, the variation of the reflectivity intensity over the range of meteorological interest necessitates the use of log Z_e instead of Z_e.

Therefore, the categories of intensity refer to log Z_e rounded to the lower whole integer. These categories are the integers that appear in the B-scan configuration of Figure 2.2.

Severe weather activity consists of heavy precipitation in the form of heavy rain and/or damaging hail along with strong winds and severe turbulence. Of the two, heavy precipitation is associated with the maximum intensities in the storm cell, while severe turbulence may occur up to 15 nautical miles from the maximum intensities.

An empirical formula has been developed by Marshall and Palmer (1) which is representative for most rains and gives a relationship between the rainfall rate R (mm/hr) and the equivalent radar reflectivity factor Z_e (mm^6/m^3).

$$Z_e = 200\ R^{1.6}\ . \tag{2.13}$$

Table 2.2 gives the rainfall rate for various categories of intensity in the absense of hail.

TABLE 2.2

RAINFALL RATE VERSUS REFLECTIVITY FACTOR

Z_e (mm^6/m^3)	R (in/hr)
10^1	0.0066
10^2	0.0256
10^3	0.175
10^4	0.454
10^5	1.82
10^6	8.04

In a study by Ward, et al. (19) it was found that eighty-five percent of hail occurrences in Oklahoma are associated with equivalent radar reflectivity factors Z_e greater than 10^5 mm^6/m^3. Whenever Z_e is less than 10^4 mm^6/m^3, hail was rare and small. It has become common practice to consider a Z_e which is greater than or equal to 10^5 mm^6/m^3 as an indication of damaging hail.

In two reports, Lee (9,10) compared measurements of turbulence and the corresponding equivalent reflectivity factors. It was found that severe turbulence is almost wholly confined to storms in which the maximum radar reflectivity factor Z_e is 10^4 mm^6/m^3 or greater. It was also found that the chance of severe turbulence is small (less than one percent) if the maximum radar reflectivity Z_e is less than 10^4 mm^6/m^3. Although the greatest turbulence is usually encountered near the area of maximum reflectivity, in 20% of the cases it occurred as far away as fifteen nautical miles.

Assigning terms such as light, moderate, and heavy to weather phenomena becomes a matter of some choice. As indicated above, the possibility is high that severe activity is associated with an intensity category of 4 or greater. Hence, those locations will be classed as "severe echo". Locations where the return power is below the minimum detectable level of the radar will be classed as "no echo". Values of intensity between "no echo" and "severe echo" will be classed as "light echo". The rectangular intensity class pattern for the intensity category pattern of Figure C.3 is given in Figure C.6. The blanks denote "no echo" locations, the L's denote "light echo" locations, and the S's denote "severe echo" locations. As before, the X's indicate locations outside of the optimum range of the radar.

Although the intensities may be classified in as many groups as there are intensity categories, it is felt that three classes contain sufficient weather information and yet allow a relatively few number of probability events needed for prediction. These probability events will be discussed in Chapter III.

Actual Weather Situations

The actual weather situations used in this study were supplied by the National Severe Storms Laboratory as representative of severe thunderstorm systems. There are two storm systems on May 5, 1967 and May 13, 1967. The storm sequence on May the 5th contains 26 patterms from 0855 CST to 1509 CST, while the storm sequence on May the 13th contains 24 patterns from 1241 CST to 1827 CST. The spacing of the patterns within each sequence was approximately fifteen minutes.

CHAPTER III

THE SUBPATTERN NEIGHBORHOOD PREDICTION PLAN

The objective of the prediction plan is to construct a rectangular prediction pattern at some future time by considering information about previous patterns within a storm sequence. Weather patterns change in two ways. First, there is an overall motion of the weather pattern, and second, there is a building and decaying of the small scale features (intensity classes). Although each change will be predicted separately, the predicted pattern motion will be used for predicting the intensity classes. The motion of the patterns will be determined using a correlation function between the patterns, while the intensity classes will be predicted using a method similar to one proposed by C.K. Chow for character recognition (3). For character recognition, the pattern is classed according to the letter it represents, while for weather prediction, the weather system itself determines the classes used for prediction.

Prediction of Pattern Motion

The use of correlation techniques for determining pattern displacement and pattern development was proposed by Hilst and Russo (6) and described in detail by J. W. Wilson (22). The method consists of superimposing two rectangular patterns taken at different times, shifting one with respect to the other and determining the best fit of the patterns. This is implemented by computing the correlation coefficient for an array of spatical lags and then selecting as the best fit those spatical distances corresponding to the maximum correlation coefficient. The lag distances associated with the maximum correlation coefficient are a measure of the linear displacement between the patterns in question. A rectangular pattern is considered as an 80 x 80 element array (See Appendix C). The rows of the array are numbered from bottom to top, and the columns are numbered from left to right. The elements of the array are integers representing intensity categories of the weather patterns. The matrix elements corresponding to locations of the weather pattern denoted by X's are assigned the value zero. A typical element of a pattern Y is y_{ij}, where y_{ij} is an integer between and including 0 and 6 representing the intensity category of the jth element of the ith row of the matrix.

Although the correlation coefficient used by Wilson was not used for the determination of pattern motion in this study, it is described here for comparison. If X and Y are two rectangular weather patterns and if x_{ij} and y_{ij} are integers representing the intensity categories ($0 \leq x_{ij}, y_{ij} \leq 6$) of the (i,j)th locations of patterns X and Y respectively, then the correlation coefficient r is given by

$$r^2(k,l) = \frac{\sum (y_{i+k,\ j+l} - \bar{X})^2}{\sum (x_{i,j} - \bar{X})^2} , \tag{3.1}$$

where $\bar{X}$ is the ensemble average of the intensity categories of pattern X. The summations of Equation 3.1 are only over those intensity pairs such that either x_{ij} or $y_{i+k,j+l}$ is not zero. The average $\bar{X}$ is determined from those intensity categories that appear in the summation of the denominator of Equation 3.1.

The motion of the patterns is determined by computing r(k,l) from Equation 3.1 for several pairs of integers, (k,l). The lag integers that correspond to the relative motion between patterns X and Y are those integers K and L such that Equation 3.2 is satisfied.

$$r(K,L) = \max_{k,l} \left\{ r(k,l) \right\} . \tag{3.2}$$

The lag integers are used to describe pattern motion in the following manner. If K and L are the lag integers, then starting with the patterns aligned, pattern X is moved K squares north (up) and L squares east (right) for the best fit as given by Equations 3.1 and 3.2. The velocity of motion would be $v = 2.5\sqrt{K^2 + L^2}/T$ knots, where T is the time between patterns in hours. The motion is due primarily to cloud movement and new cell development (3). The latter can cause the apparent velocity to be as high as 50 to 60 knots.

Instead of using a correlation coefficient to determine the lag distances, a discrete correlation function (11) is used in this paper. The correlation function between the previously defined patterns X and Y is given by

$$\varphi(k,l) = \sum_{i=1}^{80-k} \sum_{j=1}^{80-l} x_{ij} y_{i+k,\ j+l} \ . \tag{3.3}$$

Equation 3.3 is modified when either k or l is negative. The limits of the summation must be changed to insure that the range of the subscripts i, j, i+k, and j+l is not less than one nor greater than eighty. The lag integers that correspond to the motion are those integers K and L such that Equation 3.4 is satisfied.

$$\varphi(K,L) = \max_{k,l} \left\{ \varphi(k,l) \right\} \ . \tag{3.4}$$

There are several reasons for using the correlation function of Equation 3.3 instead of the correlation coefficient of Equation 3.1. Although a correlation coefficient could be used, the particular coefficient of Equation 3.1 is derived using the fact that the pattern Y is formed using a best fit polynomial regression curve (p. 243, Spiegel), which is not the case. Another reason is that since no particular use is to be made of the coefficient other than to maximize Equation 3.4, a normalized coefficient such as given in Equation 3.1 is not needed. Lastly, there are fewer operations involved in computing the correlation function of Equation 3.3 as compared with the correlation coefficient of Equation 3.1. This last reason is the most important when considering real-time computer simulation of a prediction plan using these coefficients.

Kessler and Russo (7) have reported that for a given time difference between patterns, the lag integers that correspond to the maximum correlation coefficient as determined by Equations 3.1 and 3.2 are slowly varying for a particular storm sequence. They also noted that the predicted velocity based on the immediately preceding observed velocity, the previous average velocity, or the previous velocity trend are about equally good.

Based on their findings and the fact that the lag integers K and L found for the actual storm sequences from Equations 3.3 and 3.4 are also slowly varying (See Figures 3.1 and 3.2), the predicted velocity for the prediction scheme proposed in this study was taken as the immediately preceding observed velocity. There are four time intervals for the May 13th storm sequence where the lag integers were not slowly varying: (1) 1457-1512 CST and 1512-1527 CST, (2) 1542-1556 CST and 1556-1612 CST, (3) 1657-1712 CST and 1712-1726 CST, and (4) 1712-1726 CST and 1726-1742 CST. These large variations in K and/or L were due primarily to the fact that for these time intervals most of the cloud pattern was moving out of optimum range and therefore off the PPI scan. There were no incidences where the lag integers were not slowly varying for the May 5th storm sequence.

A Prediction Plan

J. W. Wilson has proposed a prediction scheme utilizing Equations 3.1 and 3.2 (22). If $X^1, X^2, \ldots, X^n$ is a time sequence of storm patterns, then the prediction pattern $\tilde{X}^{n+1}$ for the end of the next time interval is formed as described below. The lag integers K_n and L_n are determined between patterns X^{n-1} and X^n. The prediction pattern $\tilde{X}^{n+1}$ that corresponds to the actual pattern X^{n+1} which will occur fifteen minutes later is formed by making the following assignments for all intensity classes $\tilde{x}_{ij}^{n+1}$ in pattern $\tilde{X}^{n+1}$:

$$\tilde{x}^{n+1}_{i+K_n,\ j+L_n} = x^n_{ij} . \tag{3.5}$$

where x_{ij}^n is the intensity class of location (i,j) in pattern X^n.

As an example consider the patterns for 1357 CST and 1412 CST of the May 13th storm sequence shown in Figures C.1 and C.2. The lag integers corresponding to the maximum correlation coefficient for the patterns was found to be K = 2 and L = 4. The prediction pattern for 1427

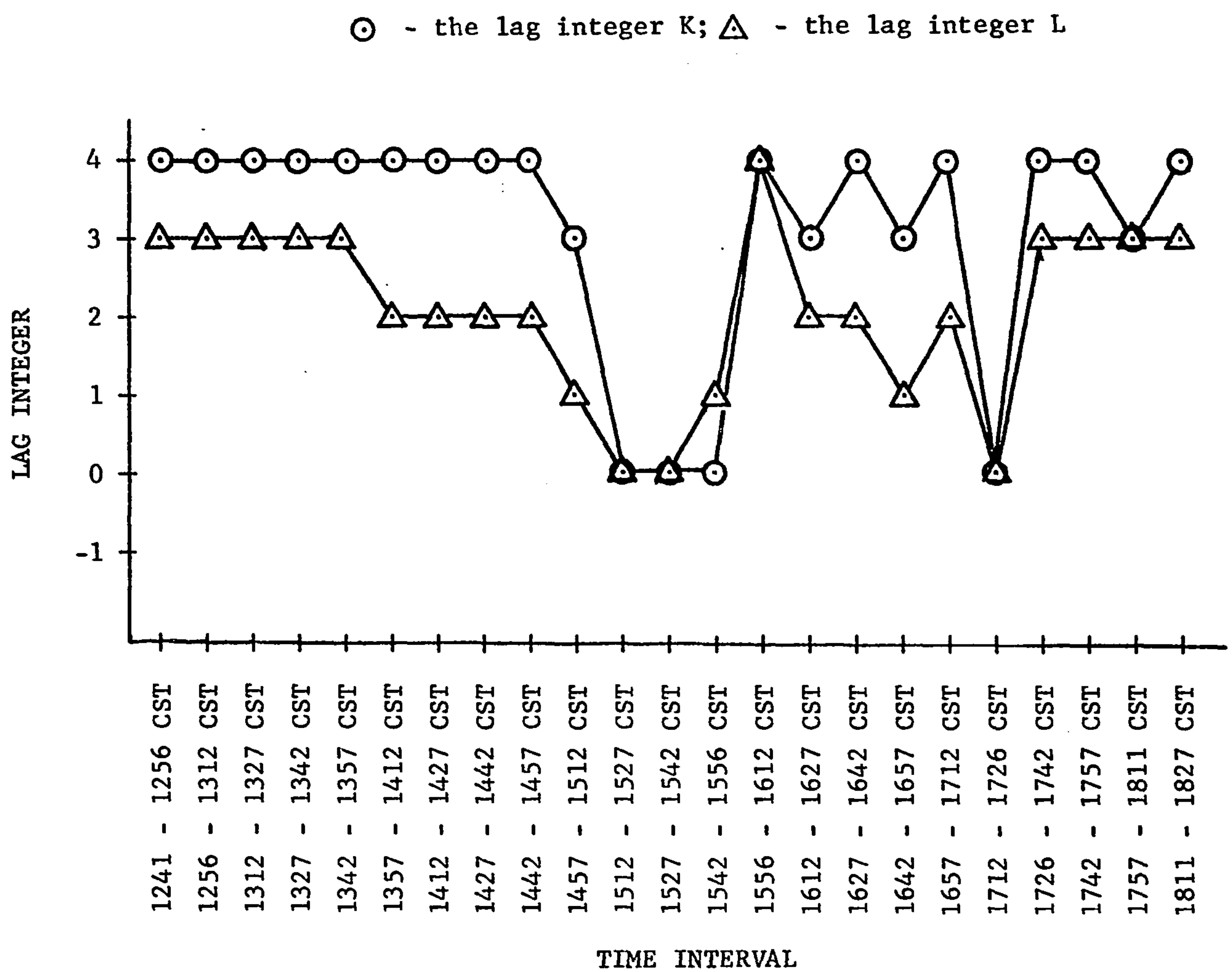

Figure 3.1. Lag integers versus time interval for May 13, 1967

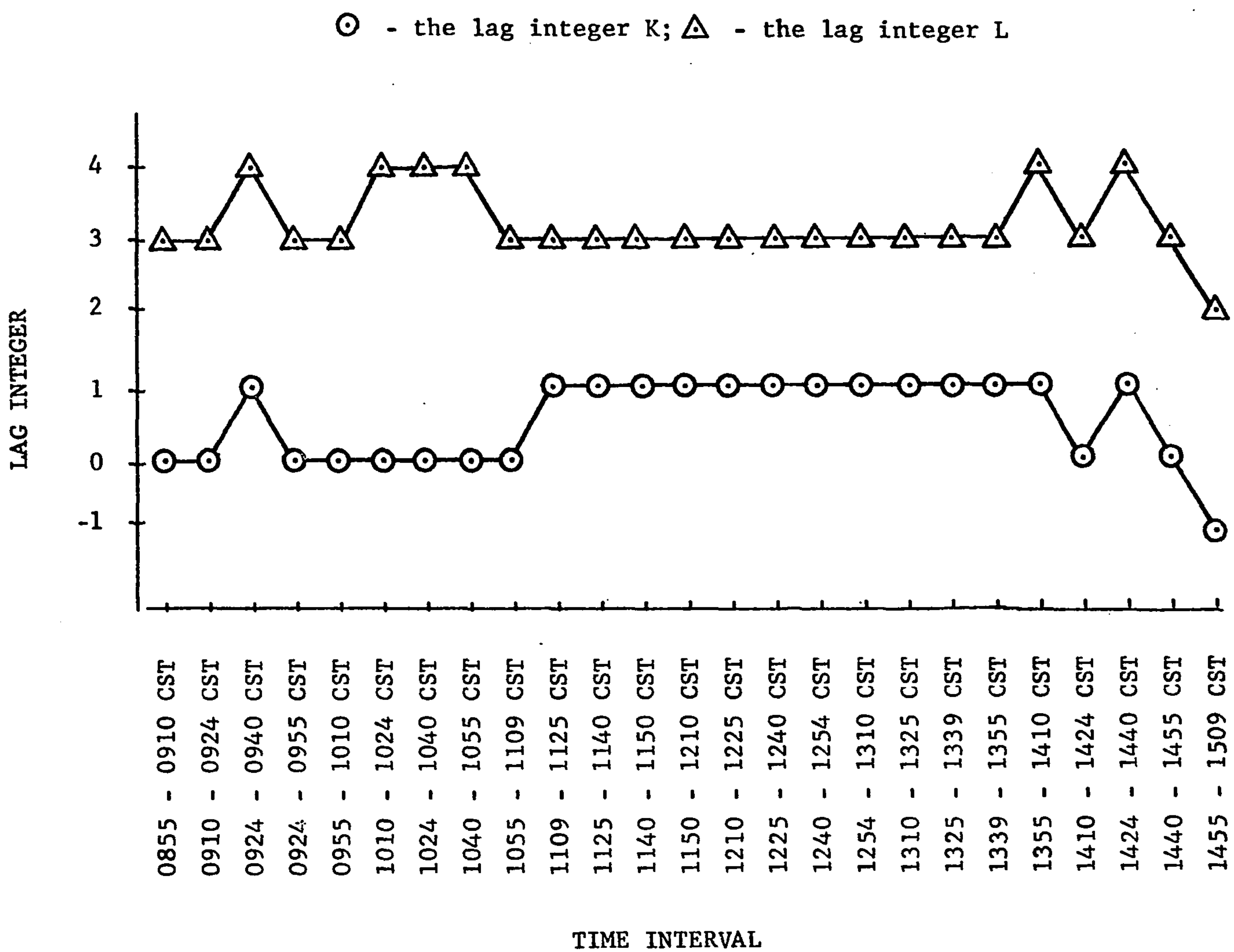

Figure 3.2. Lag integers versus time interval for May 5, 1967

CST was formed by translating the 1412 CST pattern two squares up and four squares to the right. The prediction pattern is shown in Figure C.5, while the actual pattern that occurred on May 13, 1967 at 1427 CST is shown in Figure C.3. The locations denoted by N's for the pattern in Figure C.5 and subsequent prediction patterns are those locations where no prediction was attempted. Information outside the optimum range of the preceding patterns would have been needed to form a prediction for these locations.

Although this prediction scheme is easily implemented, it's major disadvantage is that it does not predict changes in the small scale features of the weather. In order to predict these changes, more of the information contained within a pattern must be studied. It is this investigation of pattern features and the formation of a new prediction plan that forms the purpose of this paper.

A New Prediction Plan

Division into Subpatterns

From the preceding discussion, the overall pattern motion can be determined using Equations 3.3 and 3.4. This leaves the problem of determining the intensity category integer to be assigned each location within the optimum range of the prediction pattern. A possible solution to the problem is based on an intuitive knowledge of weather activity, namely, weather activity at a location is more dependent on activity at nearby locations than activity at locations remote from the given location.

The area involved in predicting the intensity category of a location may be as small as another location (Wilson's translation method) or as large as the whole pattern. The area chosen for the prediction plan of this paper is that of a square and its immediate neighbors; the area consists of nine (3 x 3) grid squares of a rectangular pattern. This can be considered as the next step in area size above that of the previously described translation plan. Each rectangular pattern is divided into approximately four thousand of these 3 x 3 overlapping subpatterns. Subpatterns containing X's are not used for prediction.

As a first approximation, it is assumed that the subpatterns have motion identical with the motion of the overall pattern. For the relative short time intervals involved, this is an adequate approximation. For larger time intervals, various storm cells may move in directions quite different from that of the overall pattern (20).

Since each subpattern contains nine squares and the intensity category for each square may vary from zero to six, there is a possibility of 7^9 distinct subpatterns. As discussed in Chapter II, the intensity categories may be grouped into three intensity classes ("no echo", "light echo", and "severe echo"). This class grouping reduces the number of distinct subpatterns to 3^9. The class grouping also reduces the sample space used to determine necessary probabilities used for prediction. The reduction of the sample space is discussed later in the chapter.

For the purpose of computation, the following correspondence between the intensity classes and the integers is convenient:

"no echo" - 1
"light echo" - 2
"severe echo" - 3

Prediction of the Intensity Classes

After the lag integers have been determined, the next step of the prediction scheme is the classification of the subpatterns. Consider the time sequence of storm patterns $X^1, X^2, \ldots, X^n$. If the lag integers between patterns X^{m-1} and X^m, $1 \leq m \leq n$, are K_m and L_m, then each subpattern of the rectangular pattern X^{m-1} is automatically classified by the weather system itself in the following manner. If W_{ij} is a subpattern having center location (i,j) in the rectangular pattern X^{m-1}, then the subpattern W_{ij} belongs to the class q, where q is the integer representing the intensity class of location $(i+K_m, j+L_m)$ of pattern X^m.

The statistical properties of the arrangement of the intensity classes within a subpatterns and the class to which the entire subpattern belongs is considered as the past history of the storm sequence $X^1, \ldots, X^n$ and is used to determine a prediction pattern $\tilde{X}^{n+1}$ for the end of the next time interval. Information about the subpattern W_{ij} of pattern X^n is used to predict the intensity class of location $(i+K_n, j+L_n)$ in the prediction pattern $\tilde{X}^{n+1}$, where K_n and L_n are the lag integers between patterns X^{n-1} and X^{n}. By considering each valid subpattern of X^{n}, a complete prediction pattern $\tilde{X}^{n+1}$ can be formed.

Along with the formulation of the actual prediction of intensity classes, a brief discussion of the decision theory used will be given (pp. 43-50, Nilsson). Basic to decision theory is the provision for a loss function. The function $\lambda(q \mid m)$, $1 \leq q, m \leq 3$, represents the loss if the machine (prediction scheme) predicts a subpattern as q, when the actual category was m. A machine that minimizes the average loss function is called a Bayes or optimum machine (15). The conditional average loss for each possible prediction q is given by

$$L_{W_{ij}}(q) = \sum_{m=1}^{3} \lambda(q \mid m) \cdot p(m \mid W_{ij}) \quad , \tag{3.6}$$

where $p(m \mid W_{ij})$ is the probability that the subpattern will belong to the class m, given that the subpattern W_{ij} occurs.

The intensity class of location (i+K, j+L) of pattern X^{n+1} is predicted to be q_o, where $L_{W_{ij}}(q_o) \geq L_{W_{ij}}(q)$ for all values of q = 1, 2, 3. There is a different conditional average loss function for each subpattern W_{ij}. By minimizing the conditional average loss for each subpattern, the value of the conditional loss averaged over all possible subpatterns is minimized.

With the use of Bayes' rule and a specified loss function, the prediction scheme can be greatly simplified. Using Bayes' rule, $p(m \mid W_{ij})$ is given by

$$p(m \mid W_{ij}) = \frac{p(W_{ij} \mid m) \cdot p(m)}{p(W_{ij})} \quad , \tag{3.7}$$

where $p(W_{ij} \mid m)$ is the probability that subpattern W_{ij} occurs, given that the subpattern belongs to the class m; $p(W_{ij} \mid m)$ is regarded as the likelihood of m with respect to W_{ij}; p(m) is the a priori probability of occurrence of class m; and $p(W_{ij})$ is the probability that W_{ij} occurs regardless of the class to which it belongs.

Using Equation 3.7, Equation 3.6 may be rewritten as

$$L_{W_{ij}}(q) = \frac{1}{p(W_{ij})} \sum_{m=1}^{3} \lambda(q|m) \cdot p(W_{ij}|m) \cdot p(m). \qquad (3.8)$$

Since $p(W_{ij})$ is a common factor in the computation of $L_{W_{ij}}(q)$, then the value of q that minimizes Equation 3.8 also minimizes

$$l_{W_{ij}}(q) = \sum_{m=1}^{3} \lambda(q|m) \cdot p(W_{ij}|m) \cdot p(m). \qquad (3.9)$$

Although many loss functions could be used, a simple as well as realistic loss function is given by

$$\lambda(q|m) = 1 - \delta_{qm} , \qquad (3.10)$$

where δ_{qm} is the Kronecker delta function. This loss function represents no loss for correctly classifying a subpattern, but gives a loss of one for misclassification.

Substituting the loss function of Equation 3.10 into Equation 3.9 yields

$$l_{W_{ij}}(q) = \sum_{\substack{m=1 \\ m \neq q}}^{3} p(W_{ij}|m) \cdot p(m) . \qquad (3.11)$$

Since $p(W_{ij}) = \sum_{m=1}^{3} p(W_{ij}|m) \cdot p(m)$, then Equation 3.11 becomes

$$l_{W_{ij}}(q) = p(W_{ij}) - p(W_{ij}|q) \cdot p(q) . \qquad (3.12)$$

Because the term $p(W_{ij})$ is common in the calculation of $l_{W_{ij}}(q)$ for each q, then minimizing Equation 3.12 can be accomplished by maximizing

$$p(W_{ij}, q) = p(W_{ij}|q) \cdot p(q) , \qquad (3.13)$$

where $p(W_{ij},q)$ is the joint probability that the subpattern W_{ij} occurs and the subpattern belongs to the class q.

If K_n and L_n are the predicted lag integers between patterns X^{n-1} and X^n, then using the special loss function of Equation 3.10 the optimum machine makes its prediction for each location of the prediction pattern $\hat{X}^{n+1}$ by the following steps:

1. Each valid subpattern W_{ij} of pattern X^n is presented to the machine.
2. The machine calculates $p(W_{ij}, q) = p(W_{ij}|q) \cdot p(q)$ for q = 1, 2,3.
3. The machine predicts that the intensity class of location (i+K, j+L) of pattern X^{n+1} will be the intensity class q_o for which $p(W_{ij}, q_o) \geq p(W_{ij}, q)$ for q = 1, 2, 3.

Conditional Probabilities

The determination of the conditional probabilities $p(W_{ij}|q)$ represents a major area of the prediction scheme. Because of the slow variation of the storm patterns, it is assumed that if the probabilities can be estimated for previous patterns, then these probabilities can be used as the predicted probabilities for the next pattern. Since the variation between storm sequences may be large (7), only patterns from the same storm sequence are used for estimating the probabilities. The number of previous patterns used to estimate the conditional probabilities varied among the different prediction schemes. This will be discussed in Chapter IV.

Consider the subpattern W_{ij} shown in Figure 3.3. The integers w_{rs} represent the intensity classes of locations (r,s), $1 \leq r,s \leq 3$, of the subpattern W_{ij} having center location (i,j) in the entire rectangular pattern.

If the intensity class w_{rs} of location (r,s) in the subpattern W_{ij} is statistically independent of the intensity classes of all other locations in the subpattern, then the conditional probability $p(W_{ij}|q)$ is given by

$$p(W_{ij}|q) = \prod_{\substack{1 \leq r \leq 3 \\ 1 \leq s \leq 3}} p(W_{rs}|q) \quad , \tag{3.14}$$

where $p(w_{rs}|q)$ is the conditional probability that the intensity class of subpattern location (r,s) is w_{rs}, given that the entire subpattern W_{ij} belongs to class q. However, for weather phenomena the intensity class for a location is not statistically independent of the intensity classes of other locations. For example, a "severe echo" location is more likely to occur next to another "severe echo" location or even a "light echo" location than next to a "no echo" location. Prompted by this observation, "nearest-neighbor dependence" similar to that proposed by C. K. Chow for character recognition (3) was assumed for the weather data.

(i+1,j-1) w_{31}	(i+1,j) w_{32}	(i+1,j+1) w_{33}
(i,j-1) w_{21}	(i,j) w_{22}	(i,j+1) w_{23}
(i-1,j-1) w_{11}	(i-1,j) w_{12}	(i-1,j+1) w_{13}

Figure 3.3. The subpattern W_{ij}

Under the assumption of "nearest-neighbor dependence" the intensity class of a location depends upon the intensity classes of its nearest neighboring grid squares and its position within the subpattern. The contional probability $p(W_{ij}|q)$ is then given by

$$p(W_{ij}|q) = \prod_{\substack{1 \leq r \leq 3 \\ 1 \leq s \leq 3}} p(w_{rs}|w_{r-1,s}, w_{r,s-1}, q) \quad , \tag{3.15}$$

where $p(w_{rs} | w_{r-1,s}; w_{r,s-1}; q)$ is the conditional probability that the intensity class of subpattern location (r,s) is w_{rs}, given that the intensity class of the nearest square below was $w_{r-1,s}$, the intensity class of the nearest square to the left was $w_{r,s-1}$, and entire subpattern W_{ij} belongs to the class q. Equation 3.15 involves only the south and west neighbors (below and to the left). The dependence on the north and east neighbors (above and to the right) are given implicitly by Equation 3.15.

Equation 3.15 extends the number of grid squares needed to form the conditional probabilities used in Equation 3.13. The extended subpattern is shown in Figure 3.4.

(i+1,j-2) w_{30}	(i+1,j-1) w_{31}	(i+1,j) w_{32}	(i+1,j+1) w_{33}
(i,j-2) w_{20}	(i,j-1) w_{21}	(i,j) w_{22}	(i,j+1) w_{23}
(i-1,j+2) w_{10}	(i-1,j-1) w_{11}	(i-1,j) w_{12}	(i-1,j+1) w_{13}
	(i-2,j-1) w_{01}	(i-2,j) w_{02}	(i-2,j+1) w_{03}

Figure 3.4 The extended subpattern W_{ij}

Extending the subpattern in this manner affects only the manner in which the subpatterns are chosen. Since the subpattern is extended to include the row w_{0j} and the column w_{i0}, care must be taken to insure these extensions do not contain an X or lie outside the 80 x 80 rectangular pattern grid.

A basic flow chart for the computer simulation used for prediction is given in Appendix A.

Probability Events

The conditional probabilities $p(w_{rs}|w_{r-1,s}; w_{r,s-1}; q)$ are determined or estimated by counting the frequency with which a probability event occurs (See Appendix B). The sample space (16) from which the conditional probabilities are determined contains all possible outcomes of the four integers w_{rs}, $w_{r-1,s}$, $w_{r,s-1}$, and q as well as the various positions w_{rs} can have within the subpattern. The sample space contains $9 \times 3^4 = 729$ points or different outcomes. Each point is denoted by the ordered 6-tuple $(r;s;w_{rs}; w_{r-1,s}; w_{r,s-1};q)$.

An event of the sample space was chosen as three points such that each point has the same value for $r,s,w_{r-1,s},w_{r,s-1}$, and q. This can be denoted as the subspace $(r;s; - ; w_{r-1,s};w_{r,s-1};q)$. There are $3^5 = 243$ disjoint events in the sample space. Each event contains three subevents, which are the various intensity classes the location (r,s) may assume within each event.

It is of interest to note that if the seven original intensity categories had not been reduced to the three intensity classes, then the sample space would contain $9 \times 7^9 = 21,609$ points or outcomes. Since each pattern contains approximately four thousand subpatterns, each containing nine squares, there are roughly $9 \times 4000 = 36,000$ occurrences per pattern. The number of occurrences should be as large as possible when compared to the size of the sample space. The primary reason for grouping the intensity categories into intensity classes was the reduction in the size of the sample space. Since the number of occurrences per pattern remains the same, then the desired improvement in the ratio of the number of occurrences to sample space size is accomplished.

CHAPTER IV

PREDICTION RESULTS, CONCLUSIONS, AND RECOMMENDATIONS

The prediction schemes given in Chapter III were applied to the two representative storm sequences. Two types of computer runs were made using the computer simulation given in Appendix A. The first type used known parameters between the two rectangular patterns X^n and X^{n+1} to "predict" the second pattern X^{n+1}. Although this first type is not actually a prediction, in that it does not use past information to predict future patterns, it does give an indication of how well the prediction schemes work, whenever the actual parameters are known for each prediction method. In the case of the subpattern neighborhood method, this can be regarded as a test of the "nearest neighborhood dependence" assumption and the use of the Bayes machine for prediction. The second type of computer run was an actual prediction, because information obtained from the previous patterns in the storm sequence $X^1, \ldots, X^{n+1}$ was used to predict a rectangular pattern $\tilde{X}^{n+1}$ that would occur fifteen minutes after pattern X^n. This was not done as an actual on-line prediction, although no reasons have been found why actual, real-time predictions could not be made.

Prediction Results Using Known Parameters

Both the translation scheme proposed by J. W. Wilson (22) and the subpattern neighborhood scheme proposed in this paper were tried for known lag integers in the case of the translation method and known lag integers and probabilities in the case of the subpattern neighborhood method.

In the case of Wilson's method, the lag integers K_{n+1} and L_{n+1} between patterns X^n and X^{n+1} were found using Equations 3.3 and 3.4. A "prediction" pattern $\tilde{X}^{n+1}$ that corresponds to the actual pattern X^{n+1} was determined by assigning the intensity class $\tilde{x}_{ij}^{n+1}$ for each location of pattern X^{n+1} as follows

$$\tilde{x}_{ij}^{n+1} = x_{i+K_{n+1}, j+L_{n+1}} \quad , \tag{4.1}$$

where x^n is an element of the rectangular pattern X^n.

For the subpattern neighborhood prediction scheme, the lag integers K_{n+1} and L_{n+1} between patterns X^n and X^{n+1} were found as for the translation method above. Using these lag integers, the frequency of occurrence for each possible outcome of the probability sample space was determined between the patterns X^n and X^{n+1}. From the frequencies of occurrence, the conditional probabilities $p(w_{rs} | w_{r-1,s};w_{r,s-1};q)$ were estimated using Method I described in Appendix B. The intensity class probabilities $p(q)$ were taken as the relative frequency of occurrences for each intensity class of pattern X^{n+1}.

The conditional probabilities $p(W_{ij}|q)$ were calculated using Equation 3.15 for each valid subpattern W_{ij} of pattern X^n. The joint probabilities $p(W_{ij},q) = p(q) \cdot p(W_{ij}|q)$ were calculated and the predicted intensity class for location $(i+K_{n+1}, j+L_{n+1})$ in the prediction pattern $\hat{X}^{n+1}$ corresponding to the actual pattern X^{n+1} was chosen to be the class q_o for which

$$p(W_{ij},q_o) = \max_q \left\{ p(W_{ij}, q) \right\} . \tag{4.2}$$

Both methods were applied to the 26 patterns of the May 5, 1967 storm sequence and the 25 patterns of the May 13, 1967 storm sequence. The actual intensity class pattern for 1427 CST, May 13, 1967, is given in Figure C.6 of Appendix C. The patterns resulting from using the translation method and subpattern neighborhood method for the 1427 CST pattern of the May 13th sequence using known parameters are given in Figures C.7 and C.8 respectively. The cumulative storm sequence results for both methods are given in Tables 4.1 and 4.2.

Since the prediction of severe weather activity is a major concern of weather forecasts, most of the discussion will be to judge the various predictions schemes on how well they predict "severe echo"

TABLE 4.1

RESULTS USING THE TRANSLATION METHOD WITH KNOWN PARAMETERS

	May 5, 1967	May 13, 1967
Actual number of "no echo" locations	107,666	111,007
Number of "no echo" locations predicted correctly	96,946	101,528
Percentage of "no echo" locations predicted correctly	90.0	91.5
Actual number of "light echo" locations	15,453	2,520
Number of "light echo" locations predicted correctly	10,541	1,415
Percentage of "light echo" locations predicted correctly	68.2	56.1
Actual number of "severe echo" locations	581	277
Number of "severe echo" locations predicted correctly	268	128
Percentage of "severe echo" locations predicted correctly	46.1	46.2
Number of "no echo" or "light echo" locations predicted as "severe echo" locations	325	144
Adjusted percent predictability of "severe echo" locations.	29.6	30.4

TABLE 4.2

RESULTS USING THE SUBPATTERN NEIGHBORHOOD METHOD WITH KNOWN PARAMETERS

	May 5, 1967	May 13, 1967
Actual number of "no echo" locations	107,666	111,007
Number of "no echo" locations predicted correctly	89,717	92,988
Percentage of "no echo" locations predicted correctly	83.5	83.1
Actual number of "light echo" locations	15,453	2,520
Number of "light echo" locations predicted correctly	4,401	1,114
Percentage of "light echo" locations predicted correctly	28.5	44.3
Actual number of "severe echo" locations	581	277
Number of "severe echo" locations predicted correctly	271	183
Percentage of "severe echo" locations predicted correctly	46.8	66.1
Number of "no echo" or "light echo" locations predicted as "severe echo" locations	56	43
Adjusted percent predictability of "severe echo" locations	42.5	57.2

locations. Two bases will be used for judging the prediction schemes. The first is simply the percent of "severe echo" locations predicted correctly. The second judges the schemes on whether or not large overprediction of "severe echo" locations occurs. This is important because overprediction not only leads to meaningless results for the first basis, but also causes a lack of confidence in real situations. The second basis is given in the rows of the tabulated results labeled "Adjusted percent predictability of 'severe echo' locations" and is computed by

$$\text{Adjusted percent predictability} = \frac{N_c}{N_a + N_o} \tag{4.3}$$

where

N_c = Number of "severe echo" locations predicted correctly

N_a = Actual number of "severe echo" locations

N_o = Number of "no echo" or "light echo" locations predicted as "severe echo" locations

For the results of Tables 4.1 and 4.2, it is clearly evident that the subpattern neighborhood scheme does much better than the translation method for the May 13th storm; however, the results for the May 5th storm are about the same for the first basis for judgement, while the adjusted percent predictability of "severe echo" is larger for the subpattern neighborhood method. A typical pattern for the May 5th storm sequence is shown in Figure C.4. The May 5th storms are larger and more widespread, while the May 13th storms are more concentrated. By separating large storms into smaller areas of activity it would appear from the results that the predictability should increase. The 66.1 percent predictability for the May 13th storm sequence is sufficient reason for using the subpattern neighborhood method as a basic scheme for weather prediction.

Also important is the predictability of severe activity in an area larger than the 6.25 square nautical mile area of one grid. The predictability in an area of nine (3 x 3) squares was determined. The results of Tables 4.3 and 4.4 show the predictability of severe activity in the larger area. The subpattern neighborhood method was markedly better than the translation method for the May 13th storm sequence, while the

TABLE 4.3

RESULTS USING THE TRANSLATION METHOD WITH KNOWN PARAMETERS IN AN AREA OF NINE SQUARES

	May 5, 1967	May 13, 1967
Actual number of "severe echo" locations	581	277
Number of areas that were correctly predicted to contain a "severe echo" location	486	224
Percentage of areas that were correctly predicted to contain a "severe echo" location	83.6	80.8
Number of areas containing only "no echo" or "light echo" locations that were incorrectly predicted to contain a "severe echo" location	98	43
Adjusted percent predictability for "severe echo" areas	71.6	70.0

TABLE 4.4

RESULTS USING THE SUBPATTERN NEIGHBORHOOD METHOD WITH KNOWN PARAMETERS IN AN AREA OF NINE SQUARES

	May 5, 1967	May 13, 1967
Actual number of "severe echo" locations	581	277
Number of areas that were correctly predicted to contain a "severe echo" location	465	243
Percentage of areas that were correctly predicted to contain a "severe echo" locations	80.0	87.7
Number of areas containing only "no echo" and "light echo" locations that were incorrectly predicted to contain a "severe echo" location	22	14
Adjusted percent predictability for "severe echo" areas	77.1	83.5

results for the May 5th storm sequence is about the same for both methods.

Results for Actual Predictions

Actual predictions using the translation method were made for the two storm sequences. This method was discussed in Chapter III and involves only a prediction of the lag integers. As discussed earlier, the predicted lag integers between an actual pattern X^n and the prediction pattern $\tilde{X}^{n+1}$ corresponding to the actual pattern X^{n+1} was taken as the computed lag integers using Equations 3.3 and 3.4 between the patterns X^{n-1} and X^n.

The prediction pattern for 1427 CST of the May 13th storm sequence is given in Figure C.10. The actual intensity class pattern that occurred on May 13th, 1967 at 1427 CST is shown in Figure C.6. The cumulative prediction results, using the translation method, are given in Table 4.5 for individual grid locations and in Table 4.6 for an area of nine squares.

Three modifications of the subpattern neighborhood scheme were used for prediction. The first, called Scheme A, consisted of estimating both the conditional probabilities $p(w_{rs}|w_{r-1,s};w_{r,s-1};q)$ and the intensity class probabilities $p(q)$ from the appropriate frequency of occurrences taken from all previous rectangular patterns in a particular storm sequence. The estimated intensity class probabilities were taken as the relative frequency for each intensity class. This was the method used to estimate the intensity probabilities for all schemes, although the number of previous patterns used in a sequence varied. The conditional probabilities for subevents of an event which had occurred were determined by Method I of Appendix B. If an event had not occurred, then the subevents were estimated to occur with a probability of zero. The predicted lag integers were found in the same manner as was used for the translation method. The predicted intensity class pattern using Scheme A for the 1427 CST pattern of the May 13th storm sequence is given in Figure C.10. The actual pattern that occurred is given in Figure C.6.

The second subpattern neighborhood method, called Scheme B, was similar to the first except for the number of patterns used and the estimation of the conditional probabilities. Instead of using all previous patterns in a storm sequence, only the immediately previous five

TABLE 4.5

ACTUAL PREDICTION RESULTS USING THE TRANSLATION METHOD FOR THE STORM SEQUENCES OF MAY 5, AND MAY 13, 1967

	May 5, 1967	May 13, 1967
Actual number of "no echo" locations	103,126	106,190
Number of "no echo" locations predicted correctly	92,530	97,170
Percentage of "no echo" locations predicted correctly	89.8	91.5
Actual number of "light echo" locations	15,085	2,411
Number of "light echo" locations predicted correctly	10,245	1,329
Percentage of "light echo" locations predicted correctly	68.0	55.1
Actual number of "severe echo" locations	541	244
Number of "severe echo" locations predicted correctly	230	255
Percentage of "severe echo" locations predicted correctly	42.5	46.3
Number of "no echo" or "light echo" locations predicted as "severe echo" locations	319	138
Adjusted percent predictability of "severe echo" locations.	68.5	73.5

TABLE 4.6

ACTUAL PREDICTION RESULTS USING THE TRANSLATION METHOD IN AN AREA OF NINE SQUARES FOR THE STORM SEQUENCES OF MAY 5, AND MAY 13, 1967

	May 5, 1967	May 13, 1967
Actual number of "severe echo" locations	541	255
Number of areas that were correctly predicted to contain a "severe echo" location	442	215
Percentage of areas that were correctly predicted to contain a "severe echo" location	81.6	83.4
Number of areas containing only "no echo" or "light echo" locations that were incorrectly predicted to contain a "severe echo" location	104	38
Adjusted percent predictability for "severe echo" areas	68.5	73.5

were used. This results in four pairs of patterns from which to count the required frequency of occurrences. For subevents of an event that had occurred at least once in the previous four pattern pairs, the conditional probabilities were estimated using Method II of Appendix B. For events that had not occurred, the conditional probabilities of each subevent was estimated as equiprobable or 1/3. The lag integers were predicted as before. The only difference between the third method, called Scheme C, and the second method was that for Scheme C the conditional probabilities for events which had occurred were estimated using Method III of Appendix B.

The cumulative results of the three prediction schemes for both storm sequences are shown in Tables 4.7 and 4.8 for individual grid locations and in Tables 4.9 and 4.10 for an area of nine squares.

Comparing the translation method (Tables 4.5 and 4.6) and the subpattern neighborhood schemes (Tables 4.7, 4.8, 4.9, and 4.10) for the predictability of "severe echo" locations shows that the translation method is better. As indicated previously for the case of known prediction parameters, the results for the May 13th storm were better than for the May 5th storm. Because of the slow variation of the lag integers (Figure 3.1) and the fact that the "nearest-neighbor dependence" assumption worked for known parameters, it can be concluded that the estimated probabilities are the primary cause of the lower predictability of severe activity for the subpattern neighborhood method.

A comparison of the three schemes of the subpattern neighborhood method was made for the best scheme to use for future study. The three subpattern neighborhood schemes use the same frequencies of occurrences to estimate the probabilities until six patterns of a sequence have occurred. This involves the prediction for four patterns since two patterns must occur before a prediction can be made. The results for the first four prediction patterns of each sequence are shown in Tables 4.11 and 4.12 for individual locations and in Tables 4.13 and 4.14 for an area of nine squares.

A comparison of the results from Tables 4.11 and 4.12 shows the methods to give about the same results. However, Scheme C, which

TABLE 4.7

ACTUAL PREDICTION RESULTS USING THE SUBPATTERN NEIGHBORHOOD SCHEMES FOR THE STORM SEQUENCE OF MAY 5, 1967

	Scheme A	Scheme B	Scheme C
Actual number of "no echo" locations	103,126	103,126	103,126
Number of "no echo" locations predicted correctly	85,599	85,628	85,661
Percentage of "no echo" locations predicted correctly	83.0	83.0	83.0
Actual number of "light echo" locations	15,085	15,085	15,085
Number of "light echo" locations predicted correctly	3,183	3,270	3,157
Percentage of "light echo" locations predicted correctly	21.2	21.7	20.9
Actual number of "severe echo" locations	541	541	541
Number of "severe echo" locations predicted correctly	112	101	74
Percentage of "severe echo" locations predicted correctly	20.7	18.7	13.7
Number of "no echo" and "light echo" locations predicted as "severe echo" locations	155	160	104
Adjusted percent predictability of "severe echo" locations	16.1	14.4	11.5

TABLE 4.8

ACTUAL PREDICTION RESULTS USING THE SUBPATTERN NEIGHBORHOOD SCHEMES FOR THE STORM SEQUENCE OF MAY 13, 1967

	Scheme A	Scheme B	Scheme C
Actual number of "no echo" locations	106,190	106,190	106,190
Number of "no echo" locations predicted correctly	88,762	88,840	88,892
Percentage of "no echo" locations predicted correctly	83.6	83.6	83.6
Actual number of "light echo" locations	2,411	2,411	2,411
Number of "light echo" locations predicted correctly	663	541	340
Percentage of "light echo" locations predicted correctly	27.5	22.4	14.1
Actual number of "severe echo" locations	255	255	255
Number of "severe echo" locations predicted correctly	83	80	46
Percentage of "severe echo" locations predicted correctly	32.6	31.4	18.0
Number of "no echo" or "light echo" locations predicted as "severe echo" locations	141	126	69
Adjusted percent predictability of "severe echo" locations	21.0	21.0	14.2

TABLE 4.9

ACTUAL PREDICTION RESULTS USING THE SUBPATTERN NEIGHBORHOOD SCHEMES IN AN AREA OF NINE SQUARES FOR THE STORM SEQUENCE OF MAY 5, 1967

	Scheme A	Scheme B	Scheme C
Actual number of "severe echo" locations	541	541	541
Number of areas that were correctly predicted to contain a "severe echo" locations	309	291	230
Percentage of areas that were correctly predicted to contain a "severe echo" location	57.1	53.8	42.5
Number of areas containing only "no echo" or "light echo" locations that were incorrectly predicted to contain a "severe echo" location	54	71	46
Adjusted percent predictability for "severe echo" areas	52.0	47.6	39.2

TABLE 4.10

ACTUAL PREDICTION RESULTS USING THE SUBPATTERN NEIGHBORHOOD SCHEMES IN AN AREA OF NINE SQUARES FOR THE STORM SEQUENCE OF MAY 13, 1967

	Scheme A	Scheme B	Scheme C
Actual number of "no echo" locations	255	255	255
Number of areas that were correctly predicted to contain a "severe echo" location	181	176	121
Percentage of areas that were correctly predicted to contain a "severe echo" location	71.0	69.0	47.5
Number of areas containing only "no echo" or "light echo" locations that were incorrectly predicted to contain a "severe echo" location	57	52	36
Adjusted percent predictability for "severe echo" areas	58.0	57.4	41.6

TABLE 4.11

ACTUAL PREDICTION RESULTS USING THE SUBPATTERN NEIGHBORHOOD SCHEMES FOR THE FIRST FOUR PREDICTION PATTERNS OF THE STORM SEQUENCE OF MAY 5, 1967

	Scheme A	Scheme B	Scheme C
Actual number of "no echo" locations	18,019	18,019	18,019
Number of "no echo" locations predicted correctly	15,257	15,262	15,266
Percentage of "no echo" locations predicted correctly	84.7	84.8	84.4
Actual number of "light echo" locations	1,662	1,662	1,662
Number of "light echo" locations predicted correctly	464	453	432
Percentage of "light echo" locations predicted correctly	26.9	27.2	26.0
Actual number of "severe echo" locations	111	111	111
Number of "severe echo" locations predicted correctly	37	39	32
Percentage of "severe echo" locations predicted correctly	33.3	35.2	28.9
Number of "no echo" or "light echo" locations predicted as "severe echo" locations	73	51	58
Adjusted percent predictability of "severe echo" locations	20.1	24.1	21.5

TABLE 4.12

ACTUAL PREDICTION RESULTS USING THE SUBPATTERN NEIGHBORHOOD SCHEMES FOR THE FIRST FOUR PREDICTION PATTERNS OF THE STORM SEQUENCE OF MAY 13, 1967

	Scheme A	Scheme B	Scheme C
Actual number of "no echo" locations	19,109	19,109	19,109
Number of "no echo" locations predicted correctly	15,584	15,603	15,620
Percentage of "no echo" locations predicted correctly	81.5	81.7	81.7
Actual number of "light echo" locations	571	571	571
Number of "light echo" locations predicted correctly	253	184	81
Percentage of "light echo" locations predicted correctly	44.3	32.2	14.2
Actual number of "severe echo" locations	112	112	112
Number of "severe echo" locations predicted correctly	31	32	13
Percentage of "severe echo" locations predicted correctly	28.0	28.6	11.6
Number of "no echo" or "light echo" locations predicted as "severe echo" locations	54	60	32
Adjusted percent predictability of "severe echo" locations	18.7	18.6	9.0

TABLE 4.13

ACTUAL PREDICTION RESULTS USING THE SUBPATTERN NEIGHBORHOOD SCHEMES FOR THE FIRST FOUR PREDICTION PATTERSN IN AN AREA OF NINE SQUARES FOR THE STORM SEQUENCE OF MAY 5, 1967

	Scheme A	Scheme B	Scheme C
Actual number of "severe echo" locations	111	111	111
Number of areas that were correctly predicted to contain a "severe echo" location	91	93	79
Percentage of areas that were correctly predicted to contain a "severe echo" locations	82.0	83.3	71.1
Number of areas containing only "no echo" or "light echo" locations that were incorrectly predicted to contain a "severe echo" location·	11	13	13
Adjusted percent predictability for "severe echo" areas	74.5	75.0	63.8

TABLE 4.14

ACTUAL PREDICTION RESULTS USING THE SUBPATTERN NEIGHBORHOOD SCHEMES FOR THE FIRST FOUR PREDICTION PATTERNS IN AN AREA OF NINE SQUARES FOR THE STORM SEQUENCE OF MAY 13, 1967

	Scheme A	Scheme B	Scheme C
Actual number of "severe echo" locations	112	112	112
Number of areas that were correctly predicted to contain a "severe echo" location	74	74	30
Percentage of areas that were correctly predicted to contain a "severe echo" location	64.2	66.2	26.8
Number of areas containing only "no echo" or "light echo" locations that were incorrectly predicted to contain a "severe echo" location	28	29	21
Adjusted percent predictability for "severe echo" areas	51.4	52.5	22.6

estimates the conditional probabilities using Method III of Appendix B, gives substantially poorer results for the May 13th storm sequence than the other two schemes. A comparison of Tables 4.13 and 4.14 gives about the same results as for Tables 4.11 and 4.12, although Scheme C gives the poorest results of all schemes for both storm sequences. This can be attributed to the manner in which the conditional probabilities are estimated. Scheme C uses Method III of Apendix B. Method III gives the largest adjustment to the conditional probabilities of subevents that have not occurred or occur infrequently. This can contribute to overadjusted probabilities and therefore cause errors in prediction. Method I, used in prediction Scheme A, gives no adjustment to nonoccurring subevents and Method II, used in prediction Scheme B, gives only minor adjustment.

Recommendations

Although the prediction results for the subpattern neighborhood schemes (Tables 4.7, 4.8, 4.9, and 4.10) were not as good as the translation method, it is not believed that the method of subpattern neighborhood prediction should be abandoned without further investigation. The prediction results for some individual patterns were quite good when compared to the translation method. The usefulness of lag integers, as proven by Wilson (22), and the results shown in Table 4.2 and 4.4 for the "nearest-neighborhood dependence" assumption and the Bayesian decision rule indicate these are all good features for a prediction scheme.

There are several possible causes for the lower than anticipated prediction results using the subpattern neighborhood method. Whether or not they are the only causes can only be conjectured for the present. One possible cause is that reducing the seven intensity categories to three intensity classes causes a loss of needed resolution, thereby reducing the predictability. It must be remembered that increasing the resolution increases the number of prediction classes which affects the size of the prediction machine. A simple increase in class size to four classes increases the sample space to $9 \times 4^4 = 2{,}304$ points. This increase in size means an increase in the time needed for prediction.

Another possible cause, which should be investigated before the size of the prediction scheme is increased, is that a basic assumption made about the weather data was invalid. The weather data was assumed to be slowly varying with time and to be independent of position within the entire pattern. If this assumption is not valid, then poor predictability can result due to an averaging of the conditional probabilities. To correct for a possible space and time variation in the probabilities, several modifications are suggested.

The first suggested modification is the subdivision of the patterns into separate cells or storm centers. This has been previously proposed (20) and is presently under study at the National Severe Storms Laboratory. This recommendation is based on the fact that the overall predictability of "severe echo" was better for the concentrated storms of May 13th. The lag integers and the frequency of occurrences used to determine the conditional probabilities could then be found for each cell. The conditional probabilities estimated from frequency of occurrences for an entire pattern are an average of the individual characteristics for each cell. Separating the pattern into cells and estimating the conditional probabilities for each cell preserves the cell's individual characteristics.

Another modification that could aid in the estimation of the conditional probabilities would be to establish whether the cell was building and decaying, then the resulting conditional probabilities estimates would be an average of the two mechanisms. However, if the frequency of occurrences were separated into sections representing increasing and decreasing parts, then using the appropriate part to estimate the conditional probabilities could overcome the misleading results caused by averaging.

A major problem in the above modifications is that the number of occurrences used to estimate the required probabilities will be reduced from those of an entire pattern. As a result, using Method I of Appendix B to estimate the conditional probabilities would lead to more conditional probabilities that are zero. These zero conditional probabilities could lead to nonpredictable intensity classes using Equation 3.15. This nonpredictability results from the fact that the conditional probabilities $p(W_{ij}|q)$ computed from Equation 3.13 would be zero for $q = 1,2,3$. Hence each joint probability $p(W_{ij}, q)$, $q = 1,2,3$, would have a probability of zero; therefore, no decision could be made as to which class to choose as most likely. This can be overcome by using a method like Method II of Apendix B, where those probabilities computed to be zero are adjusted to a small positive number.

Although elaborate procedures could be devised to estimate the probabilities, it must be remembered that as the complexity of the method increases the time required for a prediction also increases. Nothing will be gained if the prediction comes too late to be used effectively. The proposed modifications should not increase the prediction time appreciably since they only divide the large prediction scheme into smaller parts.

It is believed that the prediction scheme presented in this study could be used as a basis for future schemes which could be easily implemented for automated short-term weather forecasting.

BIBLIOGRAPHY

1. Batten, Louis J., Radar Meteorology. Chicago: The University of Chicago Press, 1959.

2. Baxter, T. L. "An Empirical Determination of the WSR-57 Radar Range Attenuation Function for Oklahoma Thunderstorms," Technical Memorandum No. 3. Norman, Oklahoma: National Severe Storms Laboratory, August 1966, pp. 1-4.

3. Chow, C. K. "A Recognition Method Using Neighbor Dependence," IRE Transactions on Electronic Computers, vol. EC-11, pp. 683-690, October 1962.

4. Davenport, W. B., Jr., and W. L. Root. Random Signals and Noise. New York: McGraw-Hill, 1958.

5. Harrington, Roger F. Time-Harmonic Electromagnetic Fields. New York: McGraw-Hill, 1961.

6. Hilst, G. R., and J. A. Russo, Jr. "An Objective Extrapolation Technique for Semi-Conservative Fields with an Application to Radar Patterns," Technical Memorandum No. 3, Contract AF30-635-14459, The Travelers Weather Research Center, Inc., 1960.

7. Kessler, Edwin III and J. A. Russo, Jr. "Statistical Properties of Weather Radar Echoes," Proceeding 10th Weather Radar Conference. Boston, Massachusetts: American Meteorological Society, 1963.

8. Kulshresthal, S. M. and K. E. Wilk. "Wave Length Dependence of the Radar Reflectivity of Water and Ice Spheres," Technical Note 3-NSSL-24. Washington, D. C.: U. S. Department of Commerce, National Severe Storms Laboratory, August 1965, pp. 33-38.

9. Lee, J. T. "Thunderstorm Turbulence and Radar Echoes, 1964 Data Studies," Technical Note 3-NSSL-24. Washington, D. C.: U. S. Department of Commerce, National Severe Storms Laboratory, August 1965, pp. 9-28.

10. Lee, J. T. "Association Between Atmospheric Turbulence and Radar Echoes in Oklahoma," Technical Memorandum No. 3. Norman, Oklahoma: National Severe Storms Laboratory, August 1966, pp. 25-30.

11. Lee, Y. W. Statistical Theory of Communication. New York: John Wiley and Sons, Inc., 1960.

12. Minsky, M. "Steps Toward Artifical Intelligence," Proceedings IRE, pp. 8-30, January 1961.

13. Newton, Charles W. and James C. Frankhauser. "Movement and Development Patterns of Convective Storms, and Forecasting the Probability of Storm Passage at a Given Location," National Severe Storms Project Report No. 22. Washington, D. C.: U. S. Department of Commerce, Weather Bureau, January 1964.

14. Nagy, George. "State of the Art in Pattern Recognition," Proceedings of the IEEE, pp. 836-862, May 1968.

15. Nils J. Nilsson. Learning Machines. New York: McGraw-Hill, 1965.

16. Reza, Fazlollah M. An Introduction to Information Theory. New York: McGraw-Hill 1961.

17. Skolnik, M. I. Introduction to Radar Systems. New York: McGraw-Hill, 1962.

18. Spiegel, M. R. Schaum's Outline of Theory and Problems of Statistics. New York: McGraw-Hill, 1961.

19. Ward, N. B., Kenneth E. Wilk, and William C. Herrman. "WSR-57 Reflectivity Measurements and Hail Observations," Technical Note 3-NSSL-24. Washington, D. C.: U. S. Department of Commerce, National Severe Storms Laboratory, August 1965, pp. 1-8.

20. Wilk, Kenneth E., "Motion and Intensity Characteristics of the Severe Thunderstorms of April 3, 1964," Technical Memorandum IERTM-NSL-29. Norman, Oklahoma: National Severe Storms Laboratory, November 1966.

21. Wilk, K. E., W. L. Watts, D. Sirmans, R. M. Lhermitte, E. Kessler, and K. C. Gray. Weather Radar Data System at the National Severe Storms Laboratory. Norman, Oklahoma: National Severe Storms Laboratory, October 1967.

22. Wilson, J. W. "Movement and Predictability of Radar Echoes," ESSA Technical Memorandum, NSSL-28. Norman, Oklahoma: National Severe Storms Laboratory, November 1966.

APPENDICES

APPENDIX A

COMPUTER SIMULATION

Although the results given in Chapter IV were determined from a computer program written in FORTRAN IV language and run on an IBM 360/40 computer, the results are computer and language independent. The simulation flow chart for the subpattern neighborhood prediction method is given in Figures A.1 and A.2.

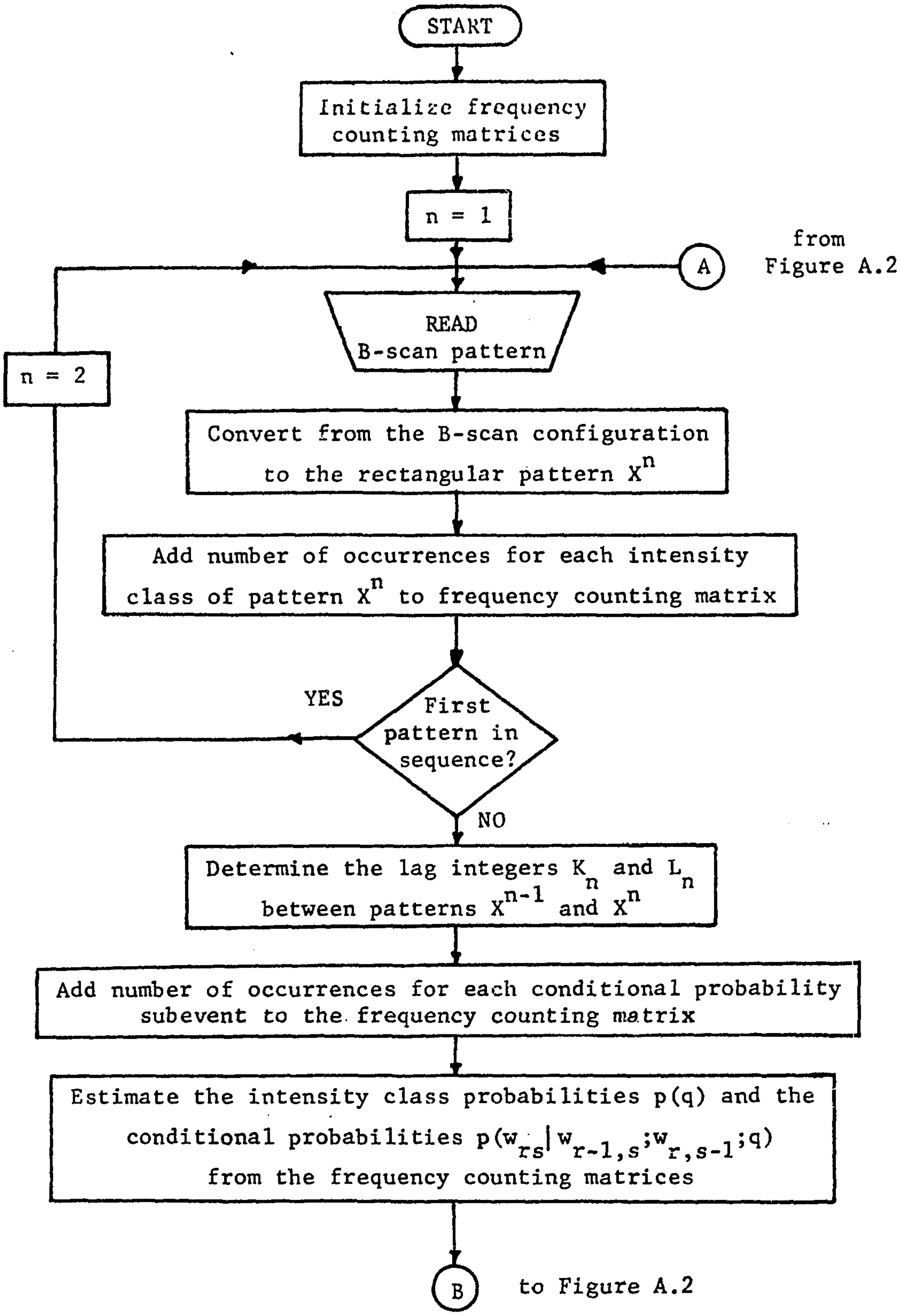

Figure A.1. Simulation flow chart of the subpattern neighborhood prediction method

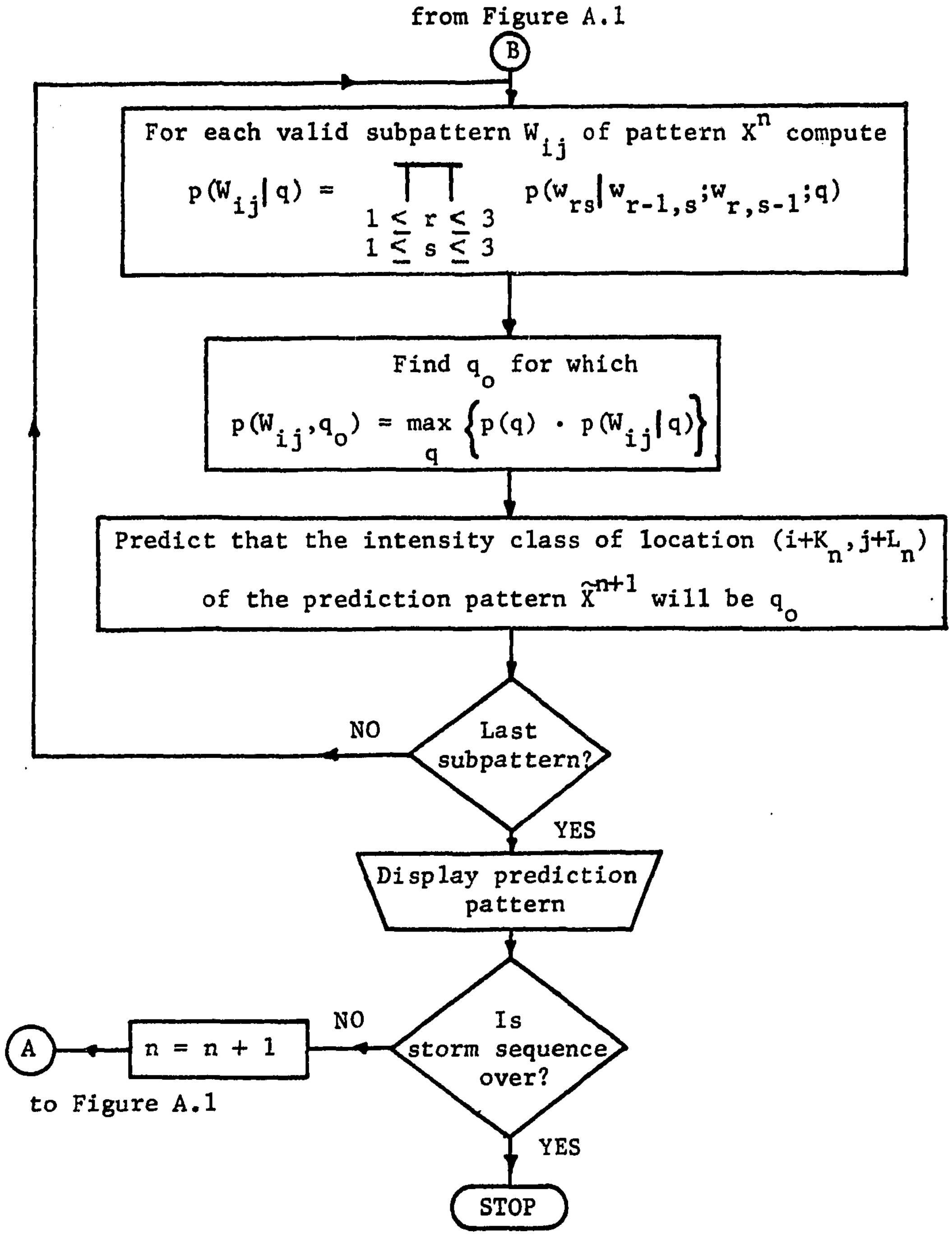

Figure A.2 Continuation of the simulation flow chart from Figure A.1

APPENDIX B

ESTIMATION OF THE CONDITIONAL PROBABILITIES

Three methods were used to estimate the conditional probabilities used for prediction. The first method used (Method I) was to estimate the conditional probabilities for a subevent simply as the relative frequency of occurrence for each subevent within the event subspace. The second method (Method II) involved a plan by C. K. Chow (3), where the probability for a subevent of an event subspace that had not occurred is assigned the value 1/3 and the probability of a subevent that had not occurred in an event subspace that had occurred is assigned the probability ϵ , where ϵ is a small positive number. The conditional probability for subevents that have occurred are estimated approximately as the relative frequency of occurrence for the subevent within the event subspace (See Examples). The third method (Method III) estimates the conditional probabilities in the following manner. If f_1, f_2, and f_3 are the frequency of occurrences for the subevents, then the probability p_i for each subevent is given by

$$p_i = \frac{f_i + 1}{F + 3} , \tag{B.1}$$

where $F = f_1 + f_2 + f_3$. Method III adjusts the probabilities more for subevents within an event subspace that has a low frequency of occurrence compared to event subspaces that occur frequently. Each method will be demonstrated for two examples.

For the examples, let $f(w_{rs} \mid w_{r-1,s};w_{r,s-1};q)$ be the frequency of occurrence of the subevent that the intensity class of location (r,s) of the subpattern is w_{rs}, the intensity class of the location below is $w_{r-1,s}$, the intensity class of the location to the left is $w_{r,s-1}$, and the entire subpattern belongs to the class q. The event is the occurrence of the intensity class $w_{r-1,s}$ in the location below, the intensity class $w_{r,s-1}$ in the location to the left, and entire subpattern belongs to the class q, independent of the intensity class location (r,s). Let T be the frequency with which an event occurs, then T is given by

$$T = \sum_{w_{rs}=1}^{3} f(w_{rs} \mid w_{r-1,s};\ w_{r,s-1};q) \qquad (B.1)$$

EXAMPLE 1

$$\begin{aligned}
f(w_{32}=1 \mid w_{22}=1;\ w_{31}=1;\ q=1) &= 11{,}762 \\
f(w_{32}=2 \mid w_{22}=1;\ w_{31}=1;\ q=1) &= 32 \\
f(w_{32}=3 \mid w_{22}=1;\ w_{31}=1;\ q=1) &= \underline{\quad 0} \\
T &= 11{,}794
\end{aligned}$$

Method I:

$$\begin{aligned}
p(w_{32}=1 \mid w_{22}=1;\ w_{31}=1;\ q=1) &= 11{,}762/11{,}794 = 0.9973 \\
p(w_{32}=2 \mid w_{22}=1;\ w_{31}=1;\ q=1) &= 32/11{,}794 = 0.0027 \\
p(w_{32}=3 \mid w_{22}=1;\ w_{31}=1;\ q=1) &= 0/11{,}794 = 0.0000
\end{aligned}$$

Method II: $\epsilon = 0.0004$

$$\begin{aligned}
p(w_{32}=1 \mid w_{22}=1;\ w_{32}=1;\ q=1) &= 0.9973 - \epsilon/2 = 0.9971 \\
p(w_{32}=2 \mid w_{22}=1;\ w_{32}=1;\ q=1) &= 0.0027 - \epsilon/2 = 0.0025 \\
p(w_{32}=3 \mid w_{22}=1;\ w_{32}=1;\ q=1) &= \epsilon = 0.0004
\end{aligned}$$

Method III:

$$\begin{aligned}
p(w_{32}=1 \mid w_{22}=1;\ w_{31}=1;\ q=1) &= \frac{11{,}762 + 1}{11{,}794 + 3} = \frac{11{,}763}{11{,}797} = 0.9971 \\
p(w_{32}=2 \mid w_{22}=1;\ w_{31}=1;\ q=1) &= \frac{32 + 1}{11{,}794 + 3} = \frac{33}{11{,}797} = 0.0028 \\
p(w_{32}=3 \mid w_{22}=1;\ w_{31}=1;\ q=1) &= \frac{0 + 1}{11{,}794 + 3} = \frac{1}{11{,}797} = 0.0001
\end{aligned}$$

EXAMPLE 2

$$\begin{aligned}
f(w_{33}=1 \mid w_{23}=2;\ w_{32}=3;\ q=2) &= 0 \\
f(w_{33}=1 \mid w_{23}=2;\ w_{32}=3;\ q=2) &= 13 \\
f(w_{33}=1 \mid w_{23}=2;\ w_{32}=3;\ q=2) &= \underline{\ 6} \\
T &= 19
\end{aligned}$$

Method I:

$$p(w_{33}=1 \mid w_{23}=2;\ w_{32}=3;\ q=2) = 0/19 = 0.0000$$
$$p(w_{33}=1 \mid w_{23}=2;\ w_{32}=3;\ q=2) = 13/19 = 0.6842$$
$$p(w_{33}=1 \mid w_{23}=2;\ w_{32}=3;\ q=2) = 6/19 = 0.3158$$

Method II: $\epsilon = 0.0004$

$$p(w_{33}=1 \mid w_{23}=2;\ w_{32}=3;\ q=2) = \epsilon = 0.0004$$
$$p(w_{33}=1 \mid w_{23}=2;\ w_{32}=3;\ q=2) = 0.6842 - \epsilon/2 = 0.4840$$
$$p(w_{33}=1 \mid w_{23}=2;\ w_{32}=3;\ q=2) = 0.3158 - \epsilon/2 = 0.3156$$

Method III:

$$p(w_{33}=1 \mid w_{23}=2;\ w_{32}=3;\ q=2) = \frac{0+1}{19+3} = \frac{1}{22} = 0.0455$$
$$p(w_{33}=1 \mid w_{23}=2;\ w_{32}=3;\ q=2) = \frac{13+1}{19+3} = \frac{14}{22} = 0.6363$$
$$p(w_{33}=1 \mid w_{23}=2;\ w_{32}=3;\ q=2) = \frac{6+1}{19+3} = \frac{7}{22} = 0.3182$$

APPENDIX C

RECTANGULAR PATTERNS

This appendix contains actual rectangular patterns for selected storms in both sequences as well as certain prediction patterns resulting from the methods discussed in Chapters III and IV.

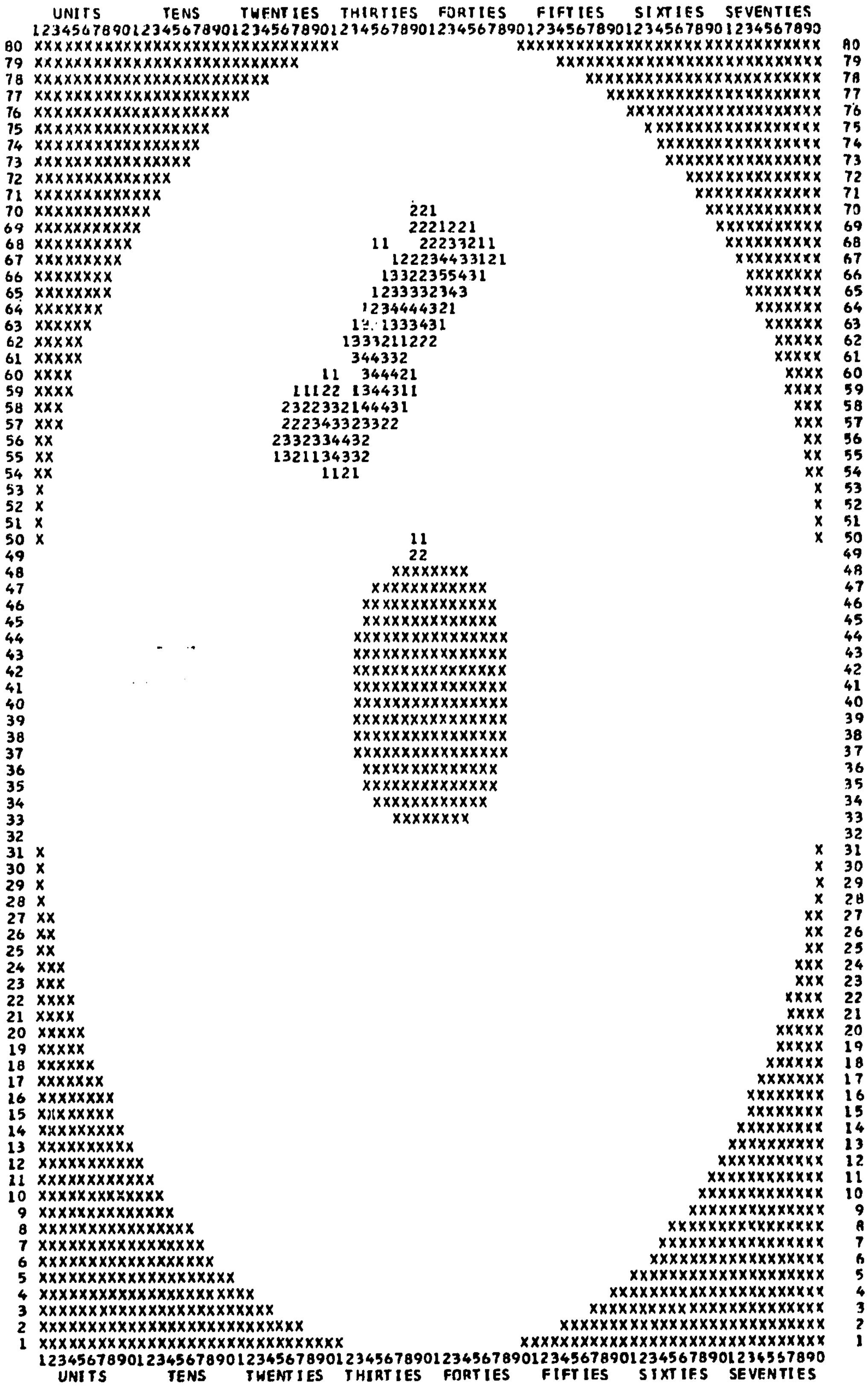

FIGURE C.1. RECTANGULAR INTENSITY CATEGORY PATTERN FOR 1357 CST, MAY 13, 1967

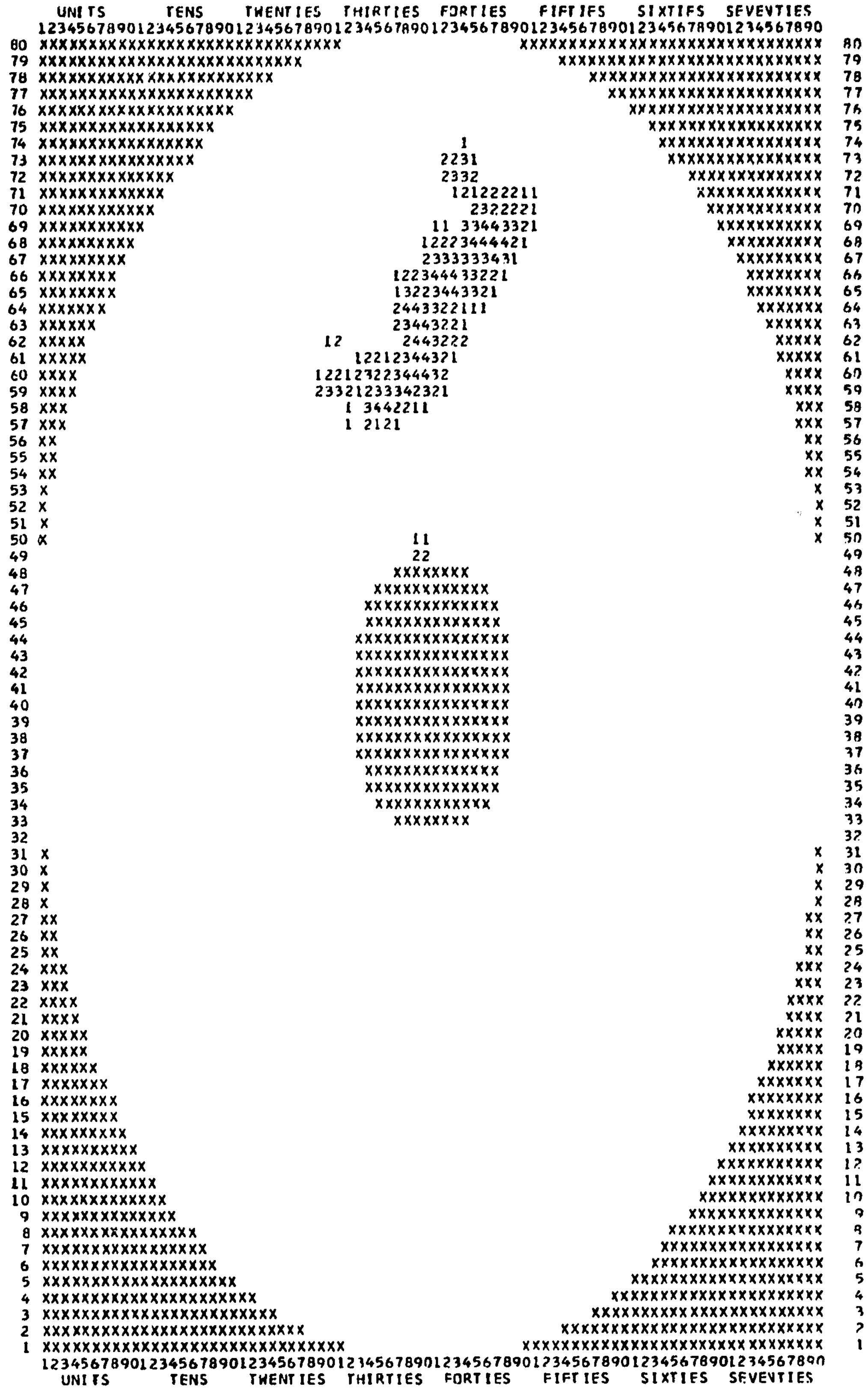

FIGURE C.2. RECTANGULAR INTENSITY CATEGORY PATTERN FOR 1412 CST, MAY 13, 1967

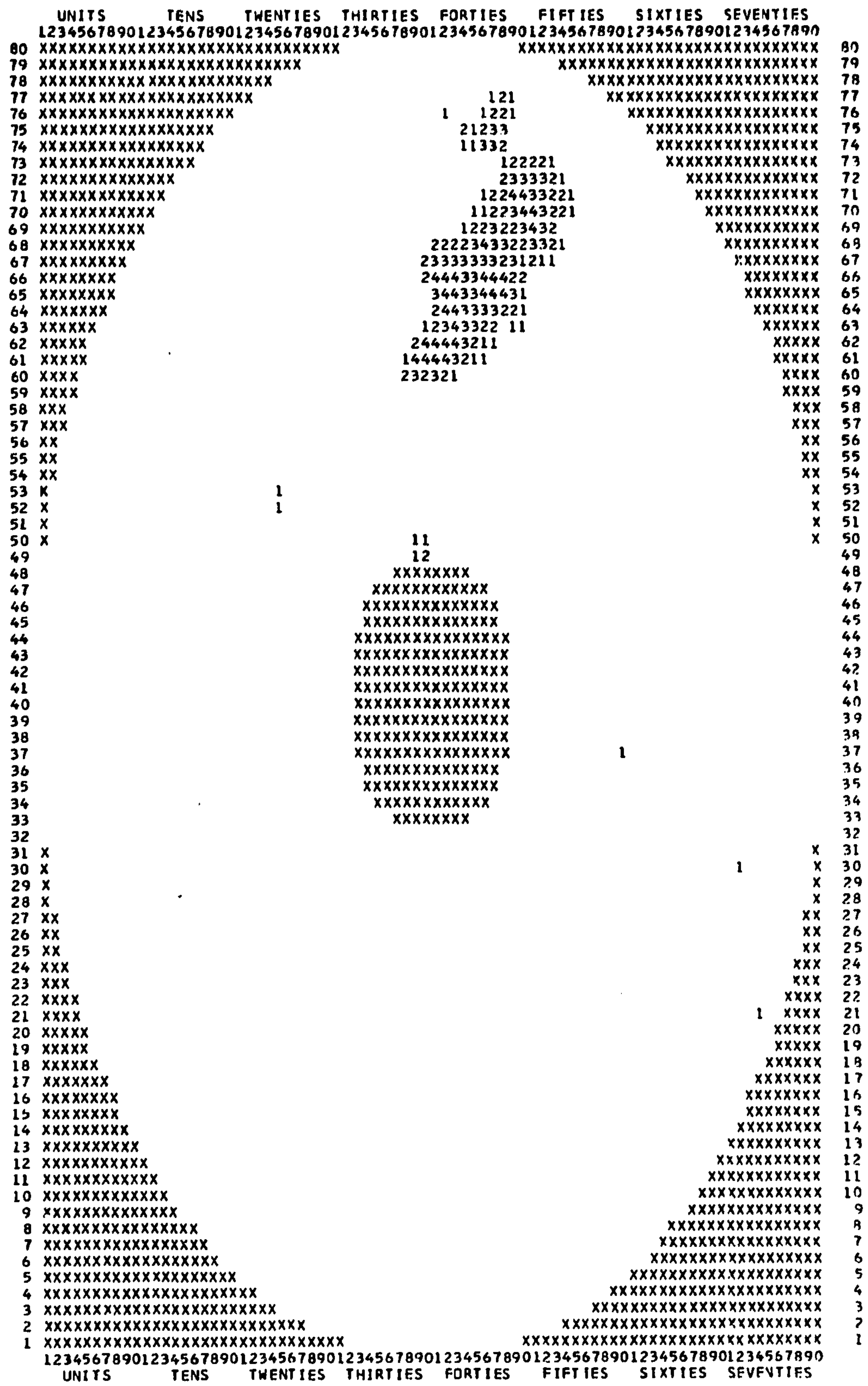

FIGURE C.3. RECTANGULAR INTENSITY CATEGORY PATTERN FOR 1427 CST, MAY 13, 1967

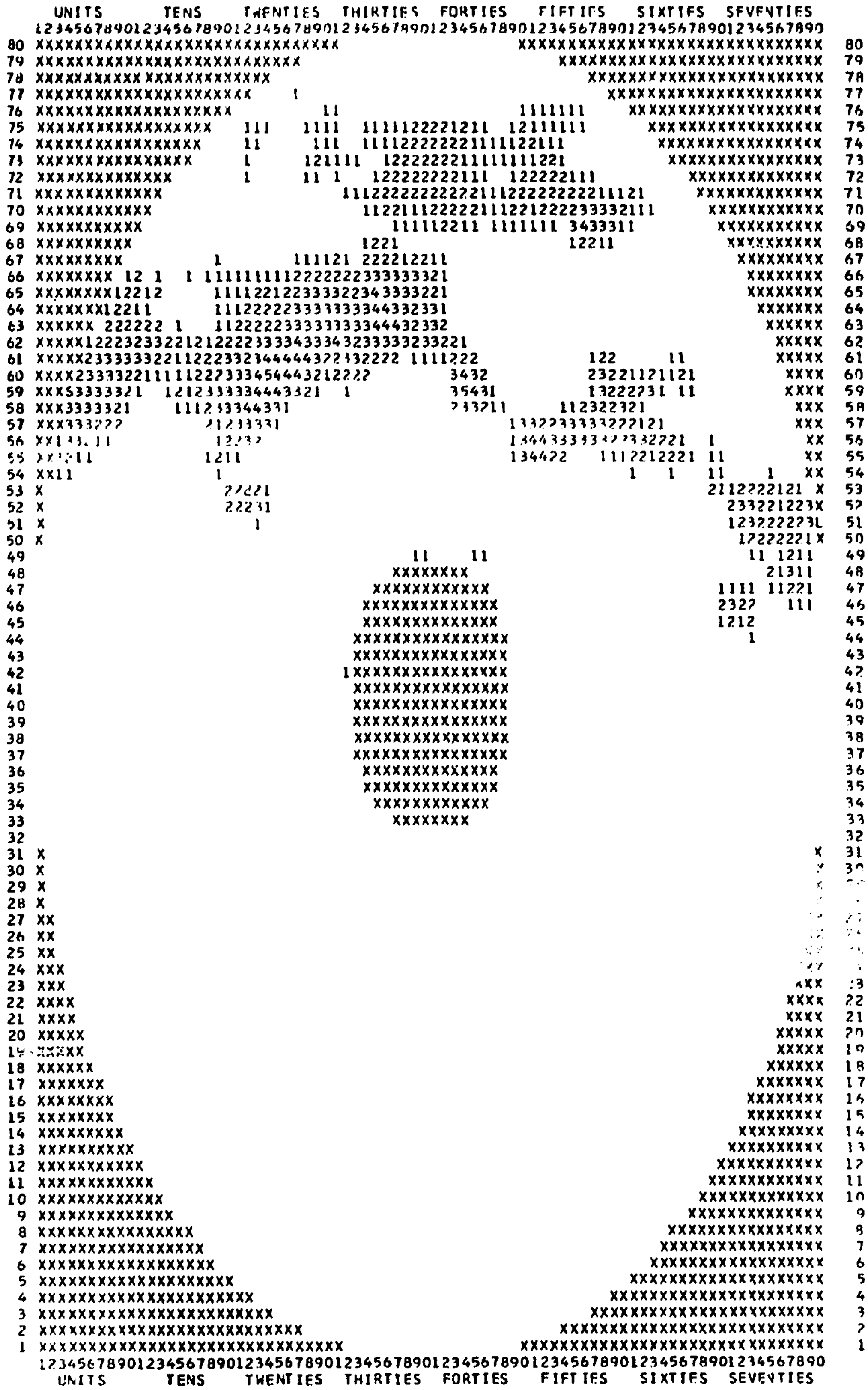

FIGURE C.4 RECTANGULAR INTENSITY CATEGORY PATTERN FOR 1325 CST, MAY 5, 1967

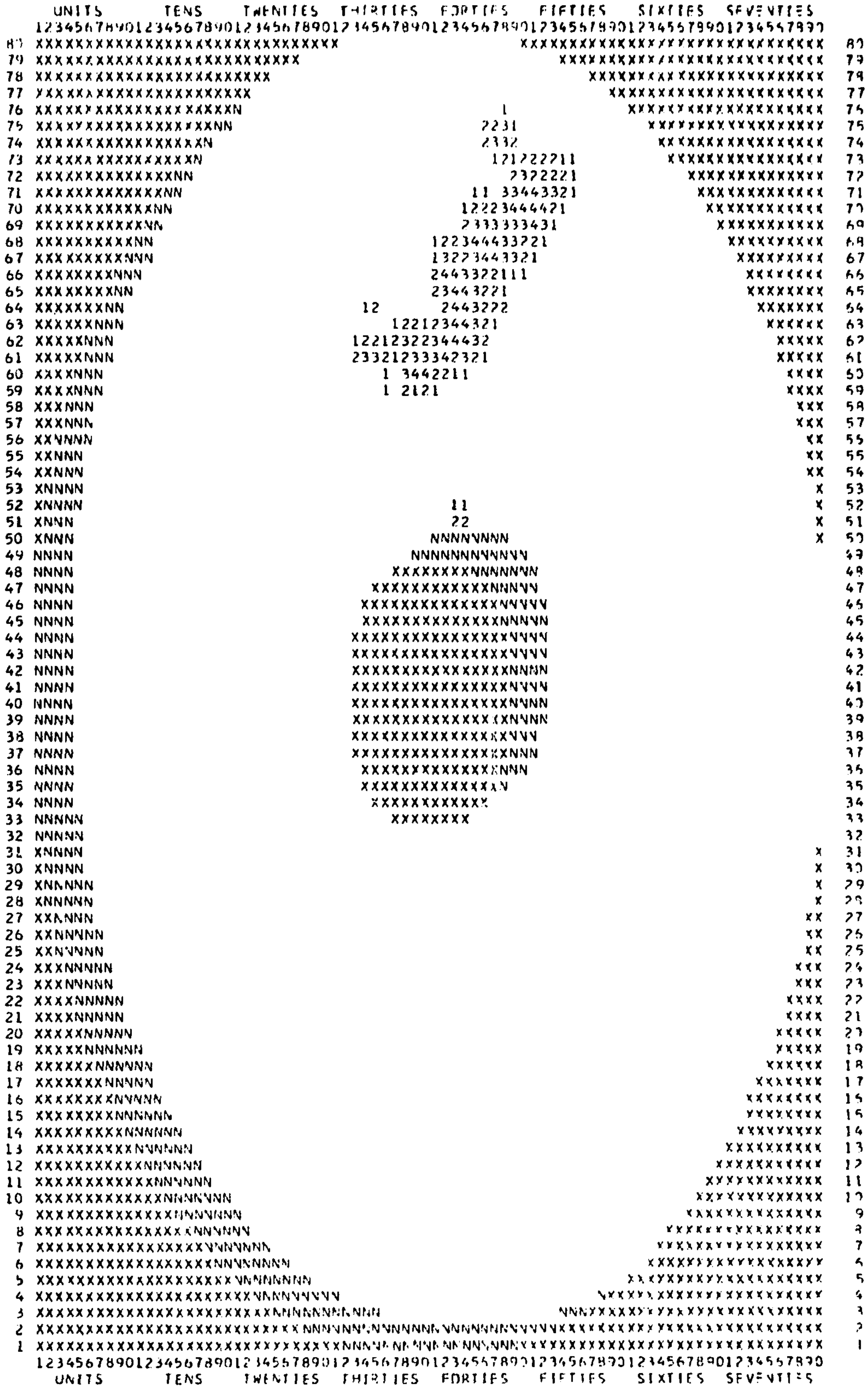

FIGURE C.5. PREDICTED INTENSITY CATEGORY PATTERN USING
THE TRANSLATION METHOD FOR 1427 CST, MAY 13, 1967

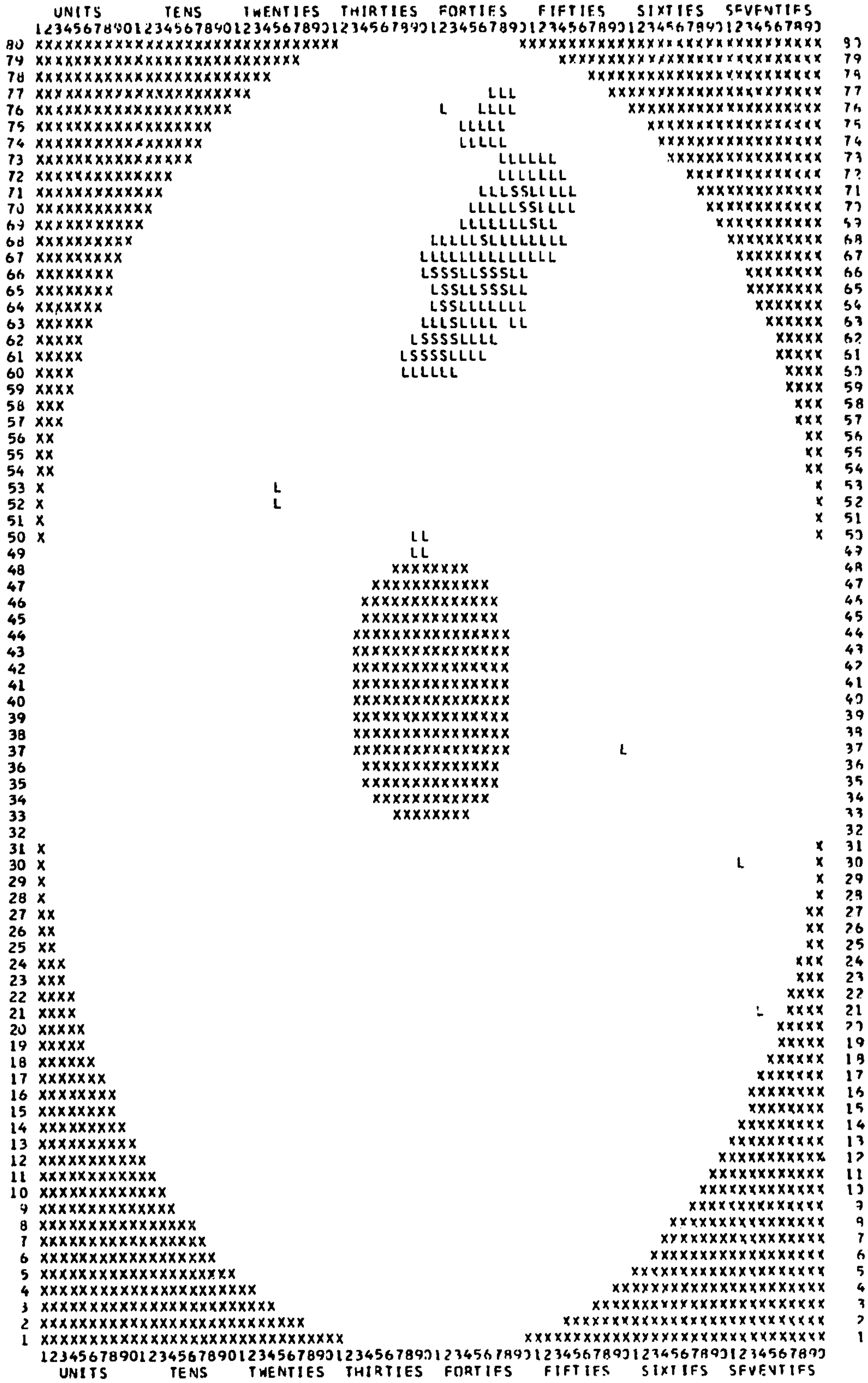

FIGURE C.6 RECTANGULAR INTENSITY CLASS PATTERN FOR 1427 CST.' MAY 13, 1967

FIGURE C.7. PATTERN RESULTING FROM USING THE TRANSLATION METHOD WITH KNOWN PARAMETERS FOR 1427 CST, MAY 13, 1967

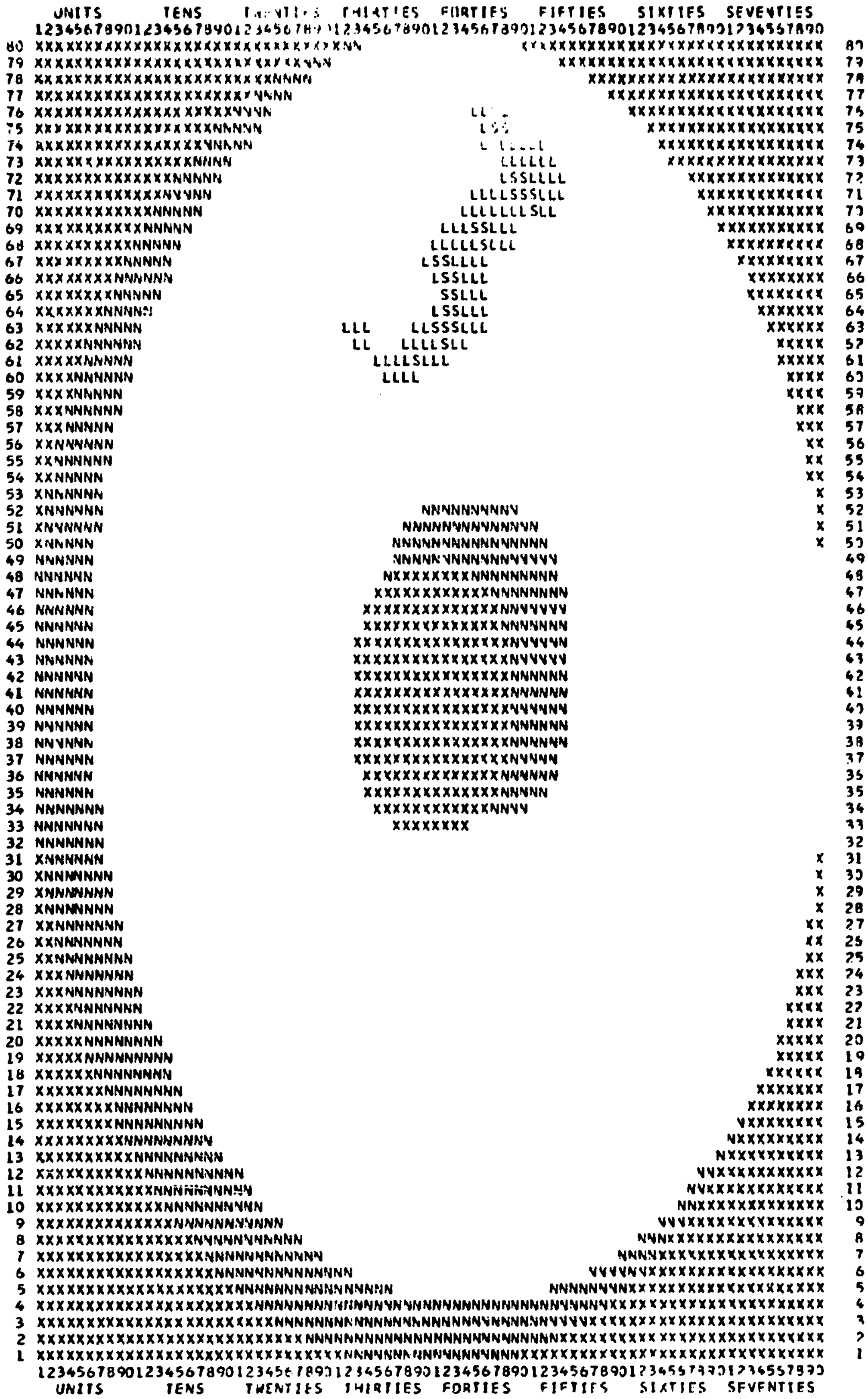

FIGURE C.8. PATTERN RESULTING FROM USING THE SUBPATTERN NEIGHBORHOOD METHOD WITH KNOWN PARAMETERS FOR 1427 CST, MAY 13, 1967

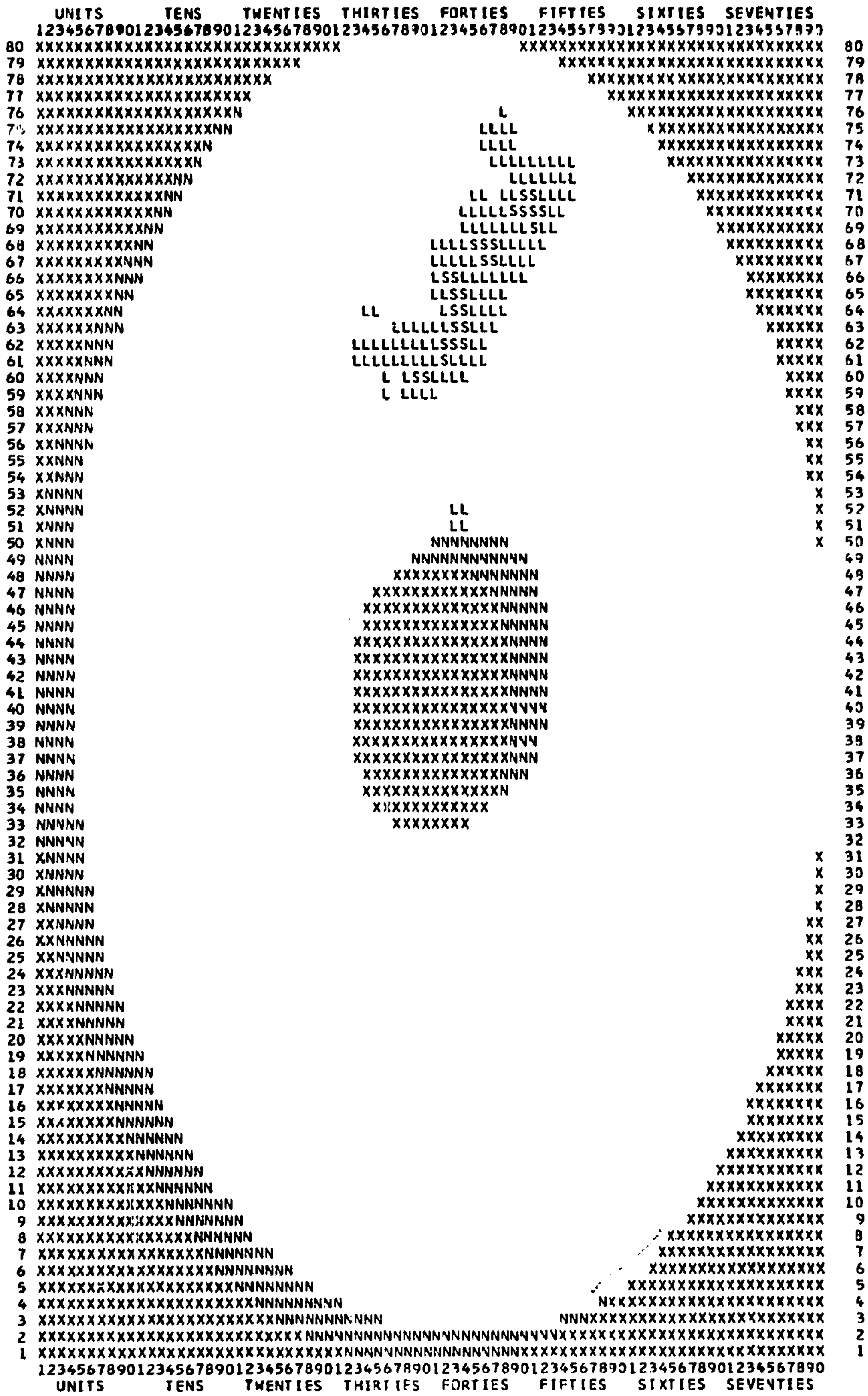

FIGURE C.9. PREDICTED INTENSITY CLASS PATTERN USING THE TRANSLATION METHOD FOR 1427 CST, MAY 13, 1967

FIGURE C.10. PREDICTED INTENSITY CLASS PATTERN USING THE SUBPATTERN NEIGHBORHOOD METHOD FOR 1427 CST, MAY 13, 1967